Computational Methods: Molecular Dynamics and Metadynamics Simulations

PLUMED 2.9.1 [1] and PLUMED-patched Gromacs2022.6 [2] were used to perform conventional molecular dynamics and metadynamics simulations, trajectory post-processing and data analysis. The ligand L^2 of [EuL^2] was modeled with CGenFF [3], and Eu was modeled with the force field developed by Qiao *et al* [4]. In this Eu force field, the coordination between Eu and other atoms is described by a Coulombic potential and a Lennard-Jones (LJ) potential. The LJ parameters for the interaction strength ($\varepsilon_{Eu} = 0.126\ kJ\ mol^{-1}$) and radius ($\sigma_{Eu} = 0.294\ nm$) of Eu were optimized such that when combined with the LJ parameters (ε_{O_W}, σ_{O_W}) of water, i.e., $\varepsilon_{Eu-O_W} = \sqrt{\varepsilon_{Eu}\varepsilon_{O_W}}$ and $\sigma_{Eu-O_W} = \left(\sigma_{Eu} + \sigma_{O_W}\right)/2$, the model can be used to reproduce the hydration free energy of Eu and the distance between Eu and water oxygen in its coordination shell.

In the present study, the interactions between Eu and other atom types were modelled with ε_{Eu-X} and σ_{Eu-O_W}, where *X* denote the pyridyl nitrogen (N_{py}), azamacrocyclic nitrogen (N_{aza}), and amide carbonyl oxygen atoms (O_{amd}). The parameters for ε_{Eu-X} were derived as $\sqrt{\varepsilon_{Eu}\varepsilon_X}$ with the parameters for ε_X taken from CGenFF, and the parameters for σ_{Eu-O_W} were adjusted to ensure that the equilibrium distances (d_{Eu-X}) between Eu and N_{py}/N_{aza}/O_{amd} during the simulations agree with those reported in the x-ray crystallography studies. The optimized parameters are $\sigma_{Eu-N_{py}} = 0.3320\ nm$, $\sigma_{Eu-N_{aza}} = 0.3824\ nm$, and $\sigma_{Eu-O_{amd}} = 0.3418\ nm$. The average d_{Eu-X} was calculated to be 0.252 nm for N_{py}, 0.285 nm for N_{aza}, and 0.247 nm for O_{amd}, consistent with the experimental values ($d_{Eu-N_{py}} = 0.254\ nm$ [5], $d_{Eu-N_{aza}} = 0.286\ nm$ [6], and $d_{Eu-O_{amd}} = 0.240\ nm$ [5]).

The initial structure of the HSA protein was retrieved from the RCSB PDB with PDB ID 2BXO. The structure was processed and protonated with the PRAS server 1.0.11[7] and all the non-standard residues were removed. CHARMM36m parameters [8] were assigned to the protein. To relax the protein in the *apo* state, it was solvated in TIP3P water with 0.15M of sodium chloride. The processed protein was minimized and pre-equilibrated under the NPT ensemble for 40 ps before proceeding. Due to the complexity of the system, we model the HSA binding of [EuL^2] in two consecutive stages: first, [EuL^2] insertion into HSA to probe which glutamate and aspartate residues could coordinate with Eu; second, Eu-carboxylate coordination was assessed, after locating the target carboxylate-containing residue.

Configuration sampling in aqueous solvent

The [EuL^2] complex was solvated in a 6 nm cubic box of TIP3P water and 0.15 M of NaCl. The system was then minimized and equilibrated, then subjected to at least 300 ns of unbiased MD simulation under the NPT ensemble using the Bussi-Donadio-Parrinello theromostat [9] and the Parrinello-Rahman barostat. The N1-C15-C14-N4 torsional angle, corresponding to one of the torsions within the 12-N-4 ring in L^2, was used as the collative variable (CV) to be biased in umbrella sampling. Twenty-one windows from -1.2 radian (-68.75 degree) to 1.2 radian (68.75 degree) at constant interval of 0.12 radian were extracted from the trajectory, using a snapshot closest to the chosen value for the later umbrella sampling. Each window was separately equilibrated first without restraint. Then, a harmonic force constant of 500 kJ/mol was

used to restrain the torsional CV, and the system was further equilibration for 2 ns, before the production sampling run of 10ns. Plumed and VMD were used to analyze the umbrella sampling trajectory. Each frame in the trajectory was reweighted using binless WHAM [10], and the 2D-FES was calculated from the weighted histograms of two torsions: (1) the N1-C15-C14-N4 torsion angle of the 12-N-4 ring; (2) the N3-C20-C19-N6 torsion angle from the nitrogen atom 3 in the 12-N-4 ring to the coordinated pyridine N atom.

Stage 1: probe insertion into human serum albumin

In an initial stage, we adapted the technique of funnel metadynamics [11] as implemented in Plumed, where a funnel-shape restraint was applied around DS-1 to restrict the movement of ligand. The funnel-shape restraint was aligned to the pre-equilibrated protein using the funnel tk plugin from FMAP [12] in VMD [13] and anchored to atom OE2 of residue 292. To define the funnel axis, we first align the original HSA-oxyphenbutazone complex onto the equilibrated unliganded HAS. Coordinates of the terminal carbon of the aligned oxyphenbutazone in DS-1 was used as the min point of the funnel axis. The max point at a distance longer than the length of [EuL^2] from the protein, and adjusted to ensure the funnel covers the whole cavity as detect by Fpocket 3.0, [14] but not pointing too far away to sample outer surface of the protein. The radius of the cylinder section of funnel was 0.2 nm, the switching point from the cone to cylinder was 5.5 nm, the angle of the cone was 0.45 radian, the lowest value of the ligand COM along funnel axis was -0.5 nm and the highest value was 7.0 nm. These parameters were set according to the suggested values in FMAP and based on preliminary tests on funnel dimensions. The [EuL^2] ligand was manually placed close to the neck of the funnel. In all the dynamical simulations, we use a timestep of 2 fs and the LINCS algorithm [15] to constrain all the bonds involving hydrogen. The Protein-[EuL^2] system was solvated in water with 0.15M of sodium chloride and minimized, followed by equilibration at 300K and 1 bar using the Berendsen thermostat and barostat with a weak harmonic restraint of 1000 kJ/mol on protein heavy atoms. The restraints were then released for an additional stage of equilibration.

Production run of funnel metadynamics had the length of 500 ns and was performed under the NPT ensemble using the Bussi-Donadio-Parrinello theromostat [9] and the Parrinello-Rahman barostat. To avoid artificial unbinding of Eu3 ion from [EuL^2], atoms with metal coordination was restrained by a harmonic force constant of 5000 kJ/mol at the distance taken from the minimized structure. The center-of-mass of the six carbon atoms in the tail phenyl group of [EuL^2] was restrained by the funnel-shape restraint with a force constant of 35,100 kJ/mol. To ensure the tail of [EuL^2] being inserted into the narrow DS-1, well-tempered metadynamics was performed with the bias potential applied on the CV defined by the distance between the center of mass of the six carbon atoms in the tail phenyl group of [EuL^2] and the center of mass of residues L219 and L238. Every 500 steps, gaussian hills were deposited along the CV with the sigma of 0.01, height 2.0, temperature 300K and a bias factor of 20.

The simulation trajectory was analyzed with Plumed, MDAnalysis [16, 17] and the FFS plugin in VMD. Relative orientation of [EuL^2] with respect to funnel axis was calculated as the angle of the dot product of two normalized vectors: (1) the vector between the Eu ion and the six carbon atoms in the tail phenyl group of [EuL^2]; (2) the funnel axis previously defined. CVs were reweighted from the metadynamics bias applied for each frame, and the free energy surface(s) was calculated along the distance between the center of mass of the six carbon atoms in the tail phenyl group of [EuL^2] and the center

of mass of residues L219 and L238. These two residues are observed to contact with the aromatic rings of oxyphenbutazone in the crystal structure, hence being used as the initial guess of the binding site of [EuL^2] phenyl group. From the free energy surface of this distance CV, we use the FFS plugin provided by the FMAP authors to estimate the binding free energy at 300K, defined the bounded state W(z) between 0.64-0.86Å, unbounded state W(ref) at 6.5Å. The FFS plugin calculate the binding free energy along a free energy surface considering the effect of the funnel-shape potential in the unbounded state, according to the following equations:

$$K_b = C^0 \pi R_{cyl}^2 \int_{site} dz e^{-\beta[W(z) - W(ref)]}$$

Where K_b is the equilibrium binding constant from the energy difference between the bounded and unbounded state, C^0 is the standard concentration of 1/1661 per cubic-Å, R_{cyl} is the radius of the cylinder part of the funnel which was 2Å (0.2-nm) in our simulation, β is $1/k_BT$ where T is the temperature of 300K in our simulation. The free energy can then be estimated with the equation $\Delta G_b^0 = -k_B T \ln(K_b)$.

Stage 2: Europium carboxylate coordination to Glu-188

From the first stage, we identified E188 to be close in space to Eu and was available for metal chelation. Hence, in the second stage we modelled the displacement of the two coordinated water molecules on the Eu ion by the carboxylate oxygens of E188. A snapshot with the shortest Eu-E188 distance from the first stage simulations was extracted from the trajectory, and solvent was removed from the snapshot. Eu-water non-bonding interactions were restored to the default. The snapshot was minimized to form the initial state of bidentate complex. The complex was then solvated into a TIP3P water box with 0.15M of NaCl, minimized and equilibrated with the same protocol as in stage 1. The equilibrated system was subjected to 450 ns of well-tempered metadynamics simulation with the bias on two CVs, (1) average distance of each E188 carboxylate oxygen to Eu, and (2) the Eu - water oxygen coordination number. Trajectories were analyzed with Plumed and visualized in VMD. The reweighted free energy along the minimum distance between E188 carboxylate oxygen and Eu in [EuL^2] was used to calculate the binding free energy contributed by the metal coordination from stage 2.

[1] The PLUMED Consortium. Promoting transparency and reproducibility in enhanced molecular simulations. *Nature Methods*, 16 (8): 670–673, 2019. ISSN 1548-7105. doi: 10.1038/s41592-019-0506-8.

[2] Mark James Abraham, Teemu Murtola, Roland Schulz, Szilárd Páll, Jeremy C. Smith, Berk Hess, and Erik Lindahl. Gromacs: High performance molecular simulations through multi-level parallelism from laptops to supercomputers. *SoftwareX*, 1–2: 19–25, 2015. ISSN 2352-7110. doi: 10.1016/j.softx.2015.06.001.

[3] K. Vanommeslaeghe, E. Hatcher, C. Acharya, S. Kundu, S. Zhong, J. Shim, E. Darian, O. Guvench, P. Lopes, I. Vorobyov, and A. D. Mackerell. Charmm general force field: A force field for drug-like molecules compatible with the charmm allâ€□atom additive biological force fields. *Journal of Computational Chemistry*, 31 (4): 671–690, July 2009. ISSN 1096-987X. doi: 10.1002/jcc.21367.

[4] Baofu Qiao, S. Skanthakumar, and L. Soderholm. Comparative charmm and amoeba simulations of lanthanide hydration energetics and experimental aqueous-solution structures. *Journal of Chemical Theory and Computation*, 14 (3): 1781–1790, February 2018. ISSN 1549-9626. doi: 10.1021/acs.jctc.7b01018.

[5] Stefania Tanase, Patricia Marques Gallego, RenÃ© de Gelder, and Wen Tian Fu. Synthesis, crystal structure and photophysical properties of europium(iii) and terbium(iii) complexes with pyridine-2,6-dicarboxamide. *Inorganica Chimica Acta*, 360 (1): 102–108, January 2007. ISSN 0020-1693. doi: 10.1016/j.ica.2006.07.115.

[6] Gerra L. Licup, Thomas J. Summers, Josiane A. Sobrinho, Ana de Bettencourtâ€Dias, and David C. Cantu. Elucidating the structure of the euâ€edta complex in solution at various protonation states. *European Journal of Inorganic Chemistry*, 27 (16), April 2024. ISSN 1099-0682. doi: 10.1002/ejic.202400042.

[7] Osita Sunday Nnyigide, Tochukwu Olunna Nnyigide, Sun-Gu Lee, and Kyu Hyun. Protein repair and analysis server: A web server to repair pdb structures, add missing heavy atoms and hydrogen atoms, and assign secondary structures by amide interactions. *Journal of Chemical Information and Modeling*, 62 (17): 4232–4246, August 2022. ISSN 1549-960X. doi: 10.1021/acs.jcim.2c00571.

[8] Jing Huang, Sarah Rauscher, Grzegorz Nawrocki, Ting Ran, Michael Feig, Bert L de Groot, Helmut GrubmÃ¼ller, and Alexander D MacKerell. Charmm36m: an improved force field for folded and intrinsically disordered proteins. *Nature Methods*, 14 (1): 71–73, November 2016. ISSN 1548-7105. doi: 10.1038/nmeth.4067.

[9] Giovanni Bussi, Davide Donadio, and Michele Parrinello. Canonical sampling through velocity rescaling. *The Journal of Chemical Physics*, 126 (1), 2007. ISSN 1089-7690. doi: 10.1063/1.2408420.

[10] Zhiqiang Tan, Emilio Gallicchio, Mauro Lapelosa, and Ronald M. Levy. Theory of binless multi-state free energy estimation with applications to protein-ligand binding. *The Journal of Chemical Physics*, 136 (14), 2012. ISSN 1089-7690. doi: 10.1063/1.3701175.

[11] Vittorio Limongelli, Massimiliano Bonomi, and Michele Parrinello. Funnel metadynamics as accurate binding free-energy method. *Proceedings of the National Academy of Sciences*, 110 (16): 6358–6363, 2013. ISSN 1091-6490. doi: 10.1073/pnas.1303186110.

[12] Stefano Raniolo and Vittorio Limongelli. Ligand binding free-energy calculations with funnel metadynamics. *Nature Protocols*, 15 (9): 2837–2866, 2020. ISSN 1750-2799. doi: 10.1038/s41596-020-0342-4.

[13] William Humphrey, Andrew Dalke, and Klaus Schulten. Vmd: Visual molecular dynamics. *Journal of Molecular Graphics*, 14 (1): 33–38, 1996. ISSN 0263-7855. doi: 10.1016/0263-7855(96)00018-5.

[14] Vincent Le Guilloux, Peter Schmidtke, and Pierre Tuffery. Fpocket: An open source platform for ligand pocket detection. *BMC Bioinformatics*, 10 (1), 2009. ISSN 1471-2105. doi: 10.1186/1471-2105-10-168.

[15] Berk Hess, Henk Bekker, Herman J. C. Berendsen, and Johannes G. E. M. Fraaije. Lincs: A linear constraint solver for molecular simulations. *Journal of Computational Chemistry*, 18 (12): 1463–1472, 1997. ISSN 1096-987X. doi: 10.1002/(sici)1096-987x(199709)18:12<1463::aid-jcc4>3.0.co;2-h.

[16] Richard Gowers, Max Linke, Jonathan Barnoud, Tyler Reddy, Manuel Melo, Sean Seyler, Jan Doma nski, David Dotson, Sébastien Buchoux, Ian Kenney, and Oliver Beckstein. Mdanalysis: A python package for the rapid analysis of molecular dynamics simulations. In *Proceedings of the 15th Python in Science Conference*, SciPy, pages 98–105. SciPy, 2016. doi: 10.25080/majora-629e541a-00e.

[17] Naveen Michaud-Agrawal, Elizabeth J. Denning, Thomas B. Woolf, and Oliver Beckstein. Mdanalysis: A toolkit for the analysis of molecular dynamics simulations.

Journal of Computational Chemistry, 32 (10): 2319–2327, 2011. ISSN 1096-987X. doi: 10.1002/jcc.21787.

Synthetic Methods and Characterisation Details

Reagents. All reagents were used without further purification as purchased. $EuCl_3.6H_2O$ was purchased from Macklin and Sigma-Aldrich (all 99.99% trace metal bases). Solvents were laboratory grade and were dried over appropriate drying agents when necessary. Air sensitive reactions were carried out under an atmosphere of nitrogen using Schlenk-line techniques.

Chromatography. Thin layer chromatography was carried out on silica plates (Merck TLC Silica gel 60 F_{254}) and visualized under UV irradiation (254/365 nm). Preparative column chromatography was performed using Biotage® Isolera™ One equipped with 200-800 nm UV-Vis detector and Biotage® Rening Cartridge – High Performance 40-63 μm. Crudes were loaded on silica gel (Bidepharm, 100-200 mesh).

Melting point measurement. Melting points were recorded using a Cole-Parmer® MP-250D-F apparatus and are uncorrected.

Nuclear magnetic resonance spectroscopy. NMR spectra were recorded on a Bruker Ultrashield 400 Plus NMR spectrometer (^{1}H NMR on 400 MHz) at 295K. The ^{1}H NMR chemical shifts were referenced to the corresponding solvent peak (7.26 for $CDCl_3$, 3.31 for CD_3OD). The following abbreviations were used to explain the multiplicities: s = singlet, d = doublet, t = triplet, dt = doublet of triplet, q = quartet, m = multiplet.

Mass spectrometry. Low-resolution mass spectra, reported as m/z, were conducted using a SCIEX 3200Q ESI mass spectrometer for monitoring reaction and determining collected fraction during purification of product. High-resolution mass spectra were obtained from a Bruker Autoflex MALDI-TOF mass spectrometer.

HPLC analysis. HPLC analyses and purifications were performed at 295 K with three different set-ups. All chromatograms were reported monitoring absorbance at 254nm and 330nm.

Agilent system. Agilent 1100 module HPLC system (Agilent Technologies, Stockport, UK), G1313A Autosampler (Micro-WPS), G1312A Binary Pump, G1315A Diode-Array Detector (DAD) and Agilent 5 HC-C18 (2) column (5 μm, 4.6 x 250 mm).

Waters system. Waters 2707 Autosampler, Water 1525 Binary HPLC Pump, Waters 2998 Photodiode Array Detector and Waters Fraction Collector III and Atlantis® T3 Prep OBD™ C18 column (5 µm, 19 × 250 mm).

Shimadzu system. Semi-preparative High Performance Liquid Chromatograph LC-20AR, LC-20AR Solvent Delivery Pump, DGU-40 Degassing unit, LH-40 Liquid Handler, SPD-M40 Photodiode Array Detector, FRC-40 Fraction Collector, CBM-40 System Controller and XBridge® Prep C18 OBD™ column (5 µm, 19 × 100 mm).

Various chromatographic systems were used for analytical and preparative HPLC:

Table S1 – HPLC conditions used for the purification of [EuL^1].

Time / min	Flow / ml min^{-1}	H_2O (0.1% TFA)	MeCN (0.1% TFA)
0	5	80	20
12	5	56	44
12.01	5	0	100
15	5	0	100
15.01	5	80	20
20	5	80	20

Table S2 – HPLC conditions used for the purification of [EuL^2].

Time / min	Flow / ml min^{-1}	H_2O (0.1% TFA)	MeCN (0.1% TFA)
0	5	80	20
16	5	59	41
16.01	5	0	100
20	5	0	100
20.01	5	80	20
25	5	80	20

Table S3 – HPLC conditions used for the purification of [EuL^3]$^+$.

Time / min	Flow / ml min^{-1}	H_2O (0.1% TFA)	MeCN (0.1% TFA)
0	5	80	20
22	5	51	49
22.01	5	0	100
25	5	0	100
25.01	5	80	20
30	5	80	20

Photophysical measurements. The ultraviolet-visible absorption spectra were measured in the range of 200-800 nm using an Agilent Technologies Cary 8454 UV-Vis spectrophotometer. The emission and excitation spectra were recorded using a Horiba FluoroMax®-4 instrument equipped with a 450 W xenon lamp operating FluorEssence (v3.8) software. Lifetime measurements were recorded using a Horiba Fluorolog®-3 instrument equipped with a 355 nm spectra-LED pulsed light source using DataStation (v2.7) software. Absorbance and ICP-MS measurements of [Eu] were made as reported elsewhere, (references 11 and 14).

CPL spectroscopy

PEM-CPL spectrometer[12]: CPL was measured with a home-built (modular) spectrometer. The excitation source was a broad band (200 – 1000 nm) laser- driven light source EQ 99 (Elliot Scientific). The excitation wavelength was selected by feeding the broadband light into an Acton SP-2155 monochromator (Princeton Instruments); the collimated light was focused into the sample cell (1 cm quartz cuvette). Sample PL emission was collected perpendicular to the excitation direction with a lens (f = 150 mm). The emission was fed through a photoelastic modulator (PEM) (Hinds Series II/FS42AA) and through a linear sheet polariser (Comar). The light was then focused into a second scanning monochromator (Acton SP-2155) and subsequently on to a photomultiplier tube (PMT) (Hamamatsu H10723 series). The detection of the CPL signal was achieved using the field modulation lock-in technique. The electronic signal from the PMT was fed into a lock-in amplifier (Hinds Instruments Signaloc Model 2100). The reference signal for the lock-in detection was provided by the PEM control unit. The monchromators, PEM control unit and lock-in amplifier were interfaced to a desktop PC and controlled by a custom-written Labview graphic user interface. The lock-in amplifier provided two signals, an AC signal corresponding to (I_L- I_R) and a DC signal corresponding to (I_L + I_R) after background subtraction. The emission dissymmetry factor was therefore readily obtained from the experimental data, as 2 AC/DC.

Spectral calibration of the scanning monochromator was performed using a Hg-Ar calibration lamp (Ocean Optics). A correction factor for the wavelength dependence of the detection system was constructed using a calibrated lamp (Ocean Optics). The measured raw data was subsequently corrected using this correction factor. The validation of the CPL detection systems was achieved using light emitting diodes (LEDs) at various emission wavelengths. The LED was mounted in the sample holder and the light from the LED was fed through a broad band polarising filter and λ/4 plate (Ocean Optics) to generate circularly polarised light. Prior to all measurements, the λ/4 plate and a LED were used to set the phase of the lock-in amplifier correctly. The emission spectra were recorded with 0.5 nm step size and the slits of the detection monochromator were set to a slit width corresponding to a spectral resolution of

0.25 nm. CPL spectra (as well as total emission spectra) were obtained through an averaging procedure of several scans. The CPL spectra were smoothed using a shape-preserving Savitzky-Golay smoothing (polynomial order 5, window size 9 with reflection at the boundaries) to reduce the influence of noise and enhance visual appearance; all calculations were carried out using raw spectral data. Analysis of smoothed vs raw data was used to help to estimate the uncertainty in the stated gem factors, which was typically ±10%.

Figures for ESI

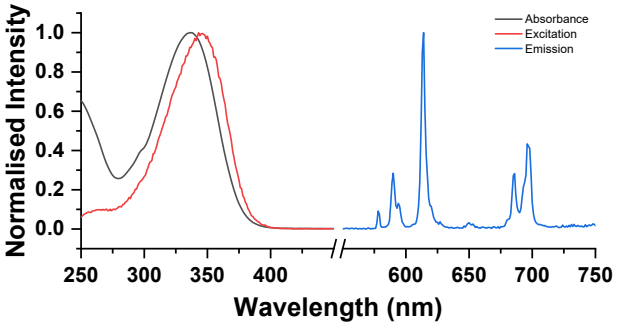

Figure S1 Absorption, excitation and emission spectra of $[EuL^3]^+$ (H_2O, 295 K, λ_{exc} 340 nm).

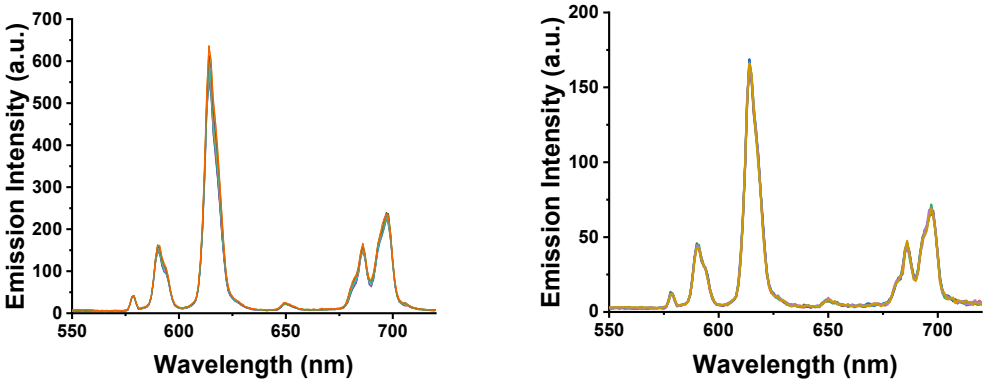

Figure S2 (*Left*): Variation of the europium (III) emission profile (upper) as a function of added bovine serum albumin and α(1)-acid glycoprotein (*Right*); $[EuL^2]$ (5 μM, λ_{exc} = 340 nm, 10 mM HEPES buffer, pH 7.4).

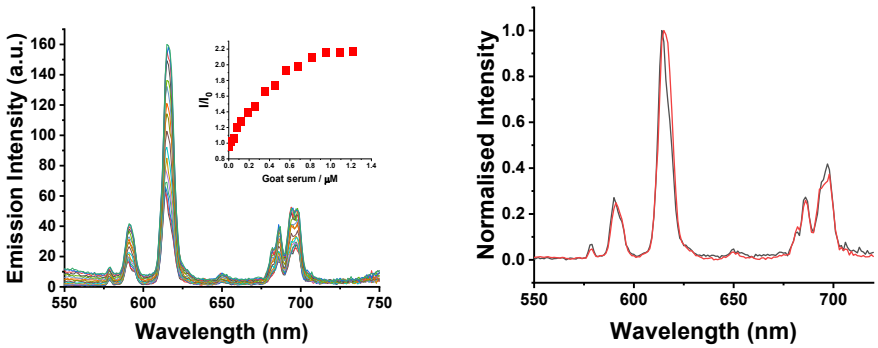

Figure S3 Variation of the europium emission spectrum (upper) upon binding of goat serum to [EuL^2] ([EuL^2] 5 μm, 10 mM HEPES, pH 7.40, 298 K, λ_{ex}=340 nm). Comparison of emission spectra(*lower*) of [EuL^2] before (*black*) and after adding goat serum.

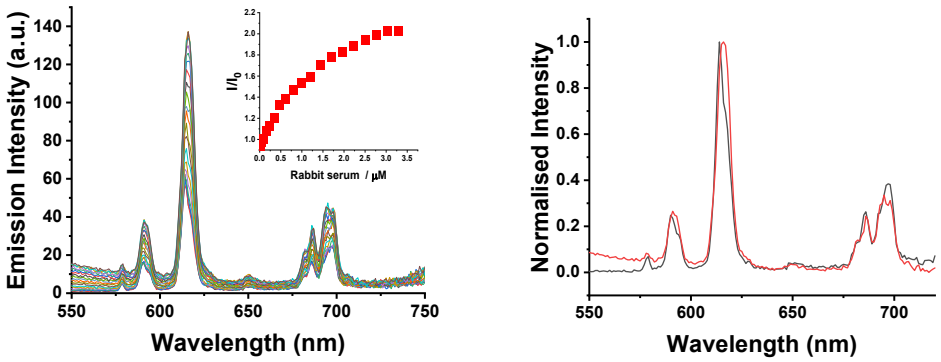

Figure S4 Variation of the europium emission spectrum (*upper*) upon binding of rabbit serum to [EuL^2] ([EuL^2] 5 μm, 10 mM HEPES, pH 7.40, 298 K, λ_{ex}=340 nm). Comparison of the emission spectral fingerprint (*lower*) of [EuL^2] before (*black*) and after adding rabbit serum (*red*).

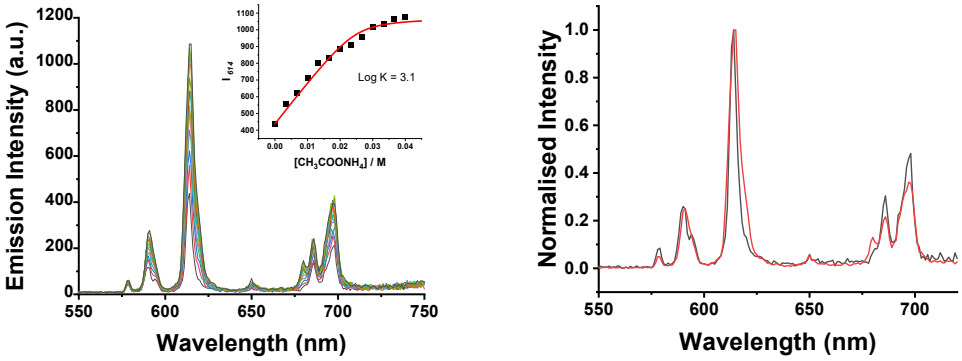

Figure S5 Variation of the europium emission spectrum (upper) on binding NH_4OAc to [EuL^2]; ([EuL^2] 5 μm, 10 mM HEPES, pH 7.40, 298 K, λ_{ex} = 340 nm). The binding affinity (log K = 3.1) was fitted assuming 1:1 binding stoichiometry. Comparison of the emission spectral fingerprint (*lower*) of [EuL^2] before (*black*) and after adding acetate (*red*).

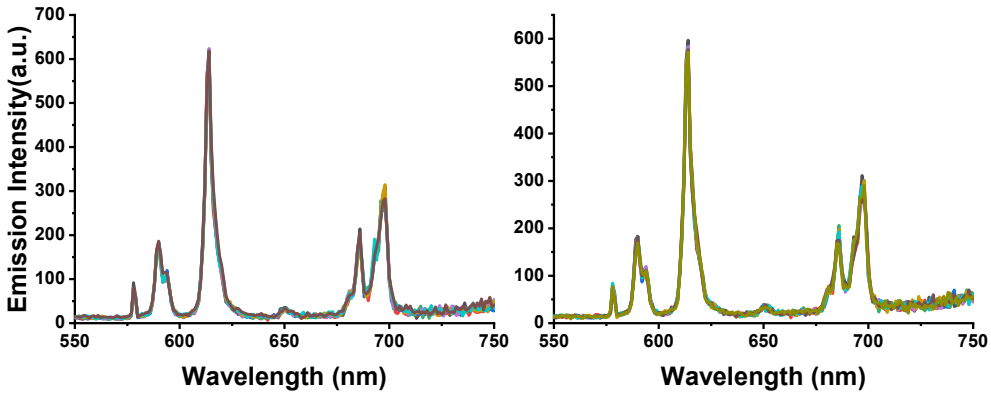

Figure S6 Variation of the europium emission spectrum of [EuL^1] on binding HSA (*left*, 0-20 μm) and BSA (*right,* 0-30 μm); ([EuL^1] 5 μm, 10 mM HEPES, pH 7.40, 298 K, λ_{ex}=330 nm).

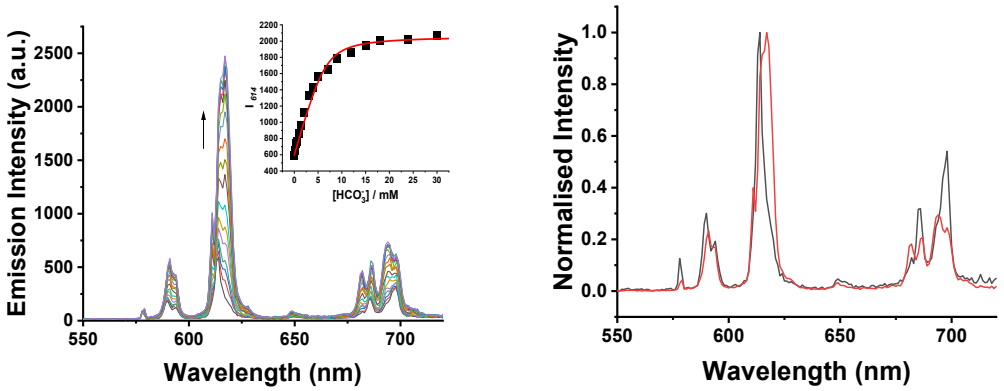

Figure S7 Variation of the europium emission spectrum upon binding of HCO_3^- to [EuL^1] ([EuL^1] 5 μm, 10 mM HEPES, pH 7.40, 298 K, λ_{ex}= 330 nm). The binding affinity (log *K* = 3.01(04) was fitted assuming 1:1 binding stoichiometry. Comparison of the emission spectral fingerprint (*lower*) of [EuL^1] before (*black*) and after adding sodium bicarbonate (*red*). Spectra have. been normalised to the most intense ΔJ = 2 transition to allow comparison.

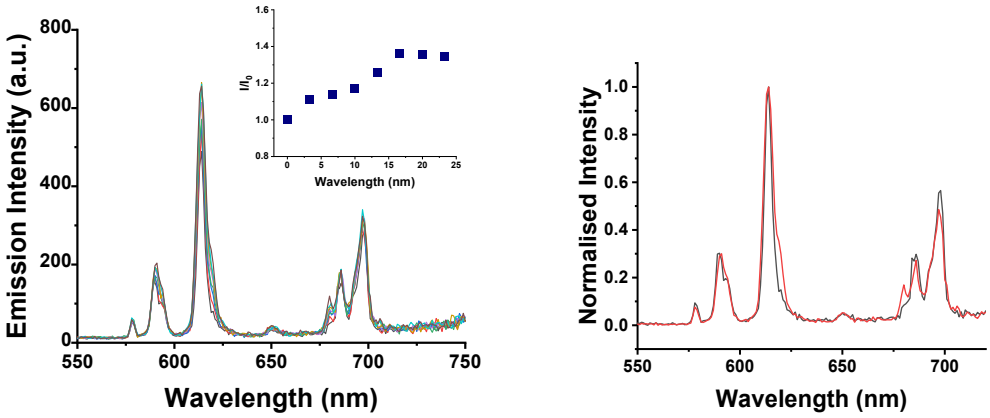

Figure S8 Variation of the europium emission spectrum (*upper*) upon binding of ammonium acetate to [EuL^1] ([EuL^1] 5 μm, 10 mM HEPES, pH 7.40, 298 K, λ_{ex}=340 nm). Comparison of the emission spectral fingerprint (*lower*) of [EuL^1] before (*black*) and after(*red*) adding ammonium acetate. No binding constant was estimated from this data set.

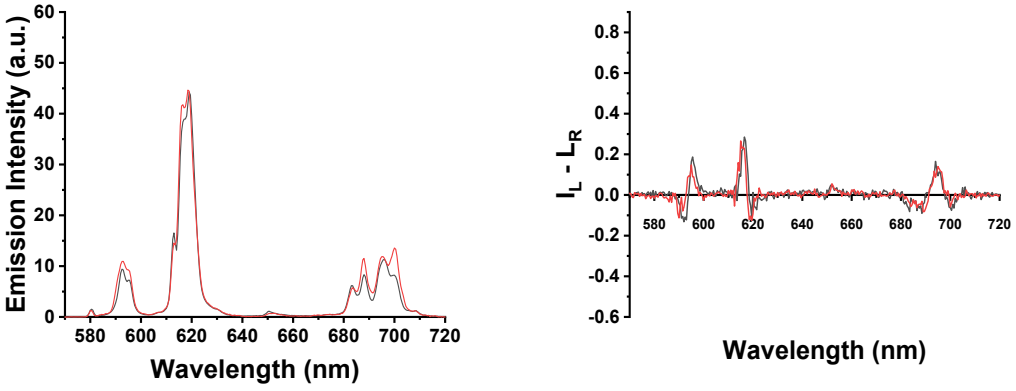

Figure S9 Total emssion (*left*) and CPL spectra following addition of excess BSA to [EuL^2]. ([EuL^2] 5 μm, 10 mM HEPES, pH 7.40, 298 K, λ_{ex}=340 nm).

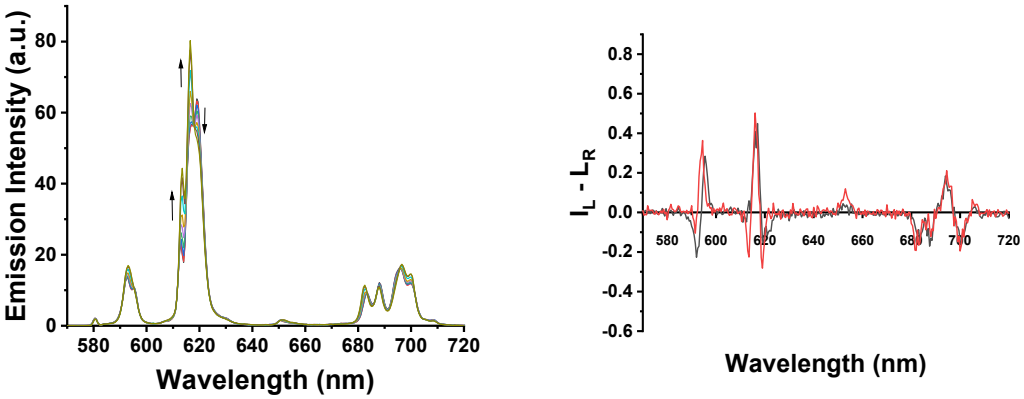

Figure S10 Changes in total emission (*left)* on binding alpha-1-AGP to [EuL^3]$^+$, and limiting CPL spectra before (*black*) and after (*red*) adding protein, (5 μM complex, 23 μM α_1-AGP, λ_{exc} = 340 nm, 10mM HEPES buffer, 295 K).

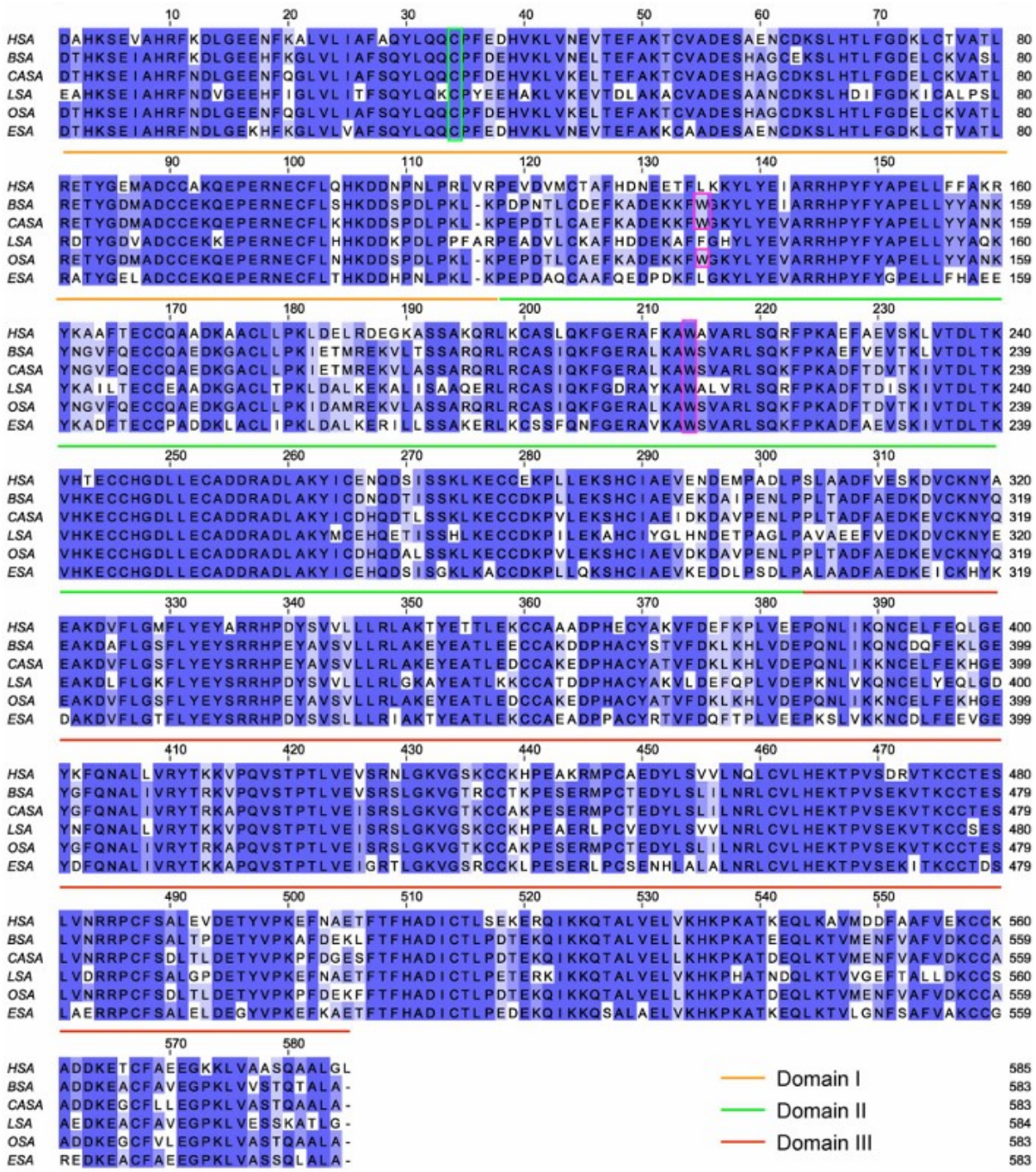

Figure S11 Multiple sequence alignment of HSA, BSA, CASA, LSA, OSA, and ESA. Orange, green, and red lines indicate domains I, II, and III, respectively [13].

Synthetic Procedures

[EuL[1]] and precursors

Compounds 1, 7, and 10 have been reported earlier in the literature, [1-3].

N-Bromoacetyl-(S)-alanine ethyl ester, 1 [1]

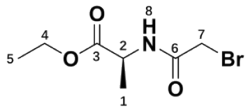

(*S*)-Alanine ethyl ester hydrochloride (1 g, 6.51 mmol) was stirred under argon at -20 ˚C in dry CH_2Cl_2 (10 ml). Triethylamine (2.72 ml, 19.5 mmol) and bromoacetyl bromide (0.9 ml, 10.4 mmol) were added and the mixture was stirred at -20 ˚C for 2 h before being allowed to gradually warm to room temperature and stirred for a further 12 h. The organic layer was washed with aq. HCl (0.1M, 30 ml) and then H_2O (4 x 25 ml), then dried over potassium carbonate and the solvent evaporated to yield a crude residue that was recrystallised from DCM / hexane to yield the product as white crystals. (0.72 g, 3.02 mmol, 47 %). **Melting point:** 42 – 43 ˚C (lit. 33 – 34 ˚C) [1]; **^{1}H-NMR** ($CDCl_3$, 400 MHz, 295 K) δ 7.03 (1H, br s, NH), 4.56 (1H, dq, H^2), 4.23 (2H, q *J* 7.0, CH_2O), 3.88 (2H, s, CH_2Br), 1.45 (3H, *J* 7.0, CH_3), 1.28 (3H, t, *J* 7.0, CH_3). **^{13}C NMR** ($CDCl_3$, 400 MHz, 295 K) δ 172.50 (C^3), 165.15 (C^6), 61.91 (C^4), 48.92 (C^2), 28.89 (C^7), 18.39 (C^1), 14.24 (C^5).

Di-tert-butyl 4,10-bis(2-((1-ethoxy-1-oxopropan-2-yl)amino)-2-oxoethyl)-1,4,7,10-tetraazacyclododecane-1,7-dicarboxylate, 2

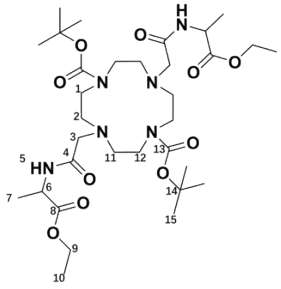

Di-tert-butyl-1,4,7,10-tetraazacyclododecane-1,7-dicarboxylate (0.16 g, 0.67 mmol) was dissolved in dry MeCN (30 ml) and bromoacetyl-(*S*)-alanine ethyl ester (0.1 g, 0.268 mmol) was added. K_2CO_3 (0.19 g, 1.34 mmol) was added and the mixture was stirred at 60 ˚C under argon for 24 h. The reaction was allowed to cool to room temperature, filtered, and the solvent was removed under reduced pressure. The desired product was isolated by column

chromatography on silica gel (DCM 3 % MeOH), as a pale-yellow, viscous oil (0.36 g, 0.52 mmol, 80 %). TLC: R_f 0.2 (silica, 3% CH_3OH in CH_2Cl_2); **^{1}H-NMR** (400 MHz, 295 K,$CDCl_3$) δ 4.56 (2H, m, H^5), 4.17 (4H, q, *J* 7.0, H^9), 3.42 (8H, br s, $H^{1,2}$), 3.28 (4H, br s, CH_2N), 2.85 (8H,br s, $H^{11,12}$), 1.44 (6H, d, H^7), 1.42 (18H, s, ^{t}Bu), 1.26 (6H, t, *J* 7.0, H^{10}). **^{13}C NMR** (101 MHz, 295 K, $CDCl_3$) δ 172.85 (C^4), 171.38 (C^8), 156.39 (C^{13}), 80.11(C^{14}), 62.23 (C^9), 61.64 (C^3), 61.35 ($C^{2,11}$), 47.98 ($C^{1,12}$), 47.76 (C^6), 28.57 (C^{15}), 18.03 ($C^{7,10}$), 14.28 ($C^{7,10}$). **MALDI-TOF MS (+)** m/z calc. for $C_{32}H_{58}N_6O_{10}$ 686.4287, found 687.4306 $[M+H]^+$

Diethyl2,2'-((2,2'-(1,4,7,10-tetraazacyclododecane-1,7-diyl)bis(acetyl))bis(azanediyl))dipropionate, 3 [1]

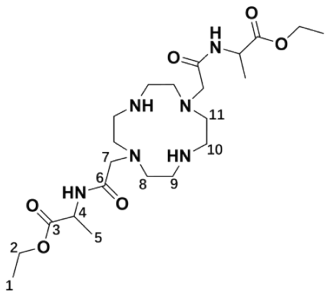

Di-tert-butyl-4,10-bis(2-((1-ethoxy-1-oxopropan-2-yl)amino)-2-oxoethyl)-1,4,7,10-tetraazacyclododecane-1,7-dicarboxylate (**2**) was dissolved in DCM:TFA (1:1, 2 ml). The mixture was stirred at room temperature for 1 h yielding a pale yellow solution. Solvent was t removed under reduced pressure to yield the product as a glassy yellow solid in quantitative yield; it was used directly in the next step without further purification. **^{1}H NMR** (400 MHz, 295 K, Methanol-d4) δ 4.49 (q, *J* 7.5 Hz, 2H, H^4), 4.17 (qq, *J* 10.8, 7.0 Hz, 4H, H^2), 3.35 – 3.54 (m, 4H), 3.29 – 2.62 (m, 16H, cyclen *NCH*), 1.38 (d, *J* 7.5 Hz, 6H, H^5), 1.26 (t, *J* 7.0 Hz, 6H, H^1). **^{13}C NMR** (101 MHz, 295 K, CD_3OD) δ 174.1 (C^6), 172.8 (C^3), 62.7($C^{2,7}$), 56.8 ($C^{8,9}$), 44.0 (C^4), 17.6 (C^5), 14.4 (C^1). **MALDI-TOF MS(+)** m/z calc. for $C_{22}H_{42}N_6O_6$ 486.3239, found 487.3169 $[M+H]^+$.

Ethyl 2-(4-iodophenoxy)acetate, 4

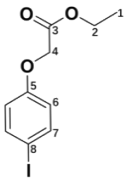

4-Iodophenol (5.00 g, 22.5 mmol) was dissolved in acetonitrile (80 mL). K_2CO_3 (4.00 g, 28.9 mmol) and ethyl bromoacetate (7.5 mL, 68.00 mmol) were added and the reaction was heated at 55 ˚C and stirred under argon for 24 h. The mixture was filtered to remove the potassium salts and the solvent was removed under reduced pressure. The residue was dissolved in CH_2Cl_2 (50 mL) and washed with water (50 mL). The aqueous layer was extracted into CH_2Cl_2 (3 x 50 mL) and the organic layers were combined, dried over $MgSO_4$, filtered and the solvent removed under reduced pressure. The crude solid was purified by flash column chromatography (silica, 2% CH_2Cl_2 in hexane) to yield a white crystalline solid (7.04 g, 99 %). TLC: Rf 0.25 (silica, 10% EtOAc in hexane); **Melting point:** 59 - 60 °C. **^{1}H NMR** (400 MHz, $CDCl_3$, 295 K) δ 7.56 (2H, d, *J* 7.5, H^6), 6.69 (2H, d, *J* 7.5, H^7), 4.58 (2H, s, H^4), 4.27 (2H, q, *J* 7.0 Hz, H^2), 1.29 (3H, t, *J* 7.0, H^1) **^{13}C NMR** (101 MHz, 295 K, $CDCl_3$) δ 168.67 (C^3), 157.90 (C^5), 138.51 (C^6), 117.19 (C^7), 84.21 (C^8), 65.55 (C^4), 61.64 (C^2), 14.30 (C^1). **MALDI-TOF MS(+)** m/z calc. for $C_{10}H_{11}IO_3$ 305.9753, found 305.9722.

Ethyl 2-(4-((2-(hydroxymethyl)pyridin-4-yl)ethynyl)phenoxy)acetate, 5

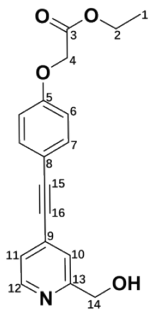

Ethyl 2-(4-iodophenoxy)acetate (**4**) (0.5 g, 1.63 mmol) was dissolved in anhydrous THF (20 mL) and the solution was degassed (three freeze-thaw cycles). (4-Ethynylpyridin-2-yl)methanol (0.17 g, 1.26 mmol) and DIPEA (3.38 mL, 2.51 mmol) were added and the solution was degassed once more. Bis(triphenylphosphine)palladium chloride (26 mg, 38 μmol) and cuprous iodide (14mg, 75 μmol) were added and the resulting brown solution was stirred at 65 °C under argon for 24 h. The solvent was removed under reduced pressure and the resulting brown oil was purified by column chromatography to give a pale yellow solid (203 mg, 40%). **Melting point:** 89 - 91°C. R_f 0.28 (silica, 5 % CH_3OH in CH_2Cl_2); **^{1}H NMR** (400 MHz, $CDCl_3$, 295 K) δ 8.52 (1H, dd, *J* 7.0, 2.5, H^{12}), 7.49 (2H, d, *J* 7.0, H^6), 7.34 (1H, d, H^{10}), 7.27 (1H, d, *J* 7.0, H^{11}), 6.92 (2H, d, *J* 7.0, H^7), 4.75 (2H, s, CH_2O), 4.64 (2H, br s, $C\underline{H}_2OH$), 4.28 (2H, q, *J* 7.0, H^2), 1.30 (3H, t, *J* 7.0, H^1). **^{13}C NMR** (101 MHz, $CDCl_3$, 295 K) δ 168.57 (C^3), 159.26 (C^5), 158.69 (C^{13}), 148.60 (C^{10}), 133.70 (C^6), 132.50 (C^9), 124.27 (C^{11}), 122.28 (C^{10}), 115.38 (C^8), 115.00 (C^7), 94.12 (C^{15}), 86.08 (C^{16}), 65.46 (C^4), 64.17(C^{14}), 61.71 (C^2), 14.30 (C^1). **MALDI-TOF MS(+)** m/z calc. for $C_{18}H_{17}NO_4$ 311.1152, found 311.1171.

Diethyl 2,2'-((2,2'-(4-((4-((4-(2-ethoxy-2-oxoethoxy)phenyl)ethynyl)pyridin-2-yl)methyl)-1,4,7,10-tetraazacyclododecane-1,7-diyl)bis(acetyl))bis(azanediyl))(2S,2'S)-dipropionate, 6

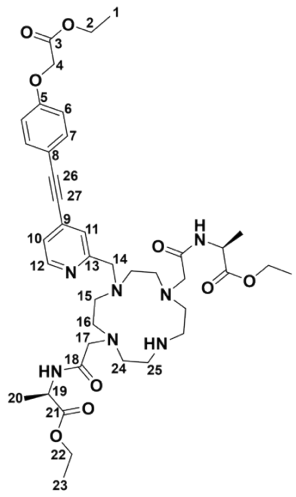

Ethyl 2-(4-((2-(hydroxymethyl)pyridin-4-yl)ethynyl)phenoxy)acetate (**5**) (50 mg, 0.16 mmol) was dissolved in anhydrous THF (2 mL) and DIPEA (0.055 mL, 0.32 mmol) was added. The mixture was stirred at 5 °C (ice/water bath) and methanesulfonic anhydride (42 mg, 0.24 mmol) was added. The reaction was allowed to warm to room temperature and stirred under nitrogen for 3 h. The solvent was removed under reduced pressure and the residue dissolved in CH_2Cl_2 (15 mL) and washed with water (15 mL). The aqueous layer was re-extracted with CH_2Cl_2 (3 x 15 mL) and the organic layers were combined, dried over $MgSO_4$, filtered and the solvent removed under reduced pressure to yield the mesylate ester as a bright yellow oil (30 mg, 50%), which was used directly in the next step without further purification. TLC: R_f 0.45 (silica, 5 % CH_3OH in CH_2Cl_2); **ESI-MS(+)** m/z calc. for $C_{19}H_{19}NO_6S$ 389.093, found 390.110 $[M+H]^+$.

(*SS*)-4,10-Bis(ethyl-N-acetyl-*S*-alanine)-1,4,7,10- tetraazacyclododecane (13 mg, 33.4 µmol) was dissolved in dry MeCN (2 ml) and the mesylate prepared freshly in the previous step (24 mg, 50 µmol) was added. DIPEA (29 µL, 0.17 mmol) was added and the mixture was stirred at 60 ˚C under argon for 24 h. The reaction was allowed to cool to room temperature. The solvent was removed under reduced pressure. The desired product was isolated by HPLC to afford a light orange glassy oil (16 mg, 43 %). **^{1}H NMR** (400 MHz, CD_3OD, 295 K) δ 8.51 (1H, s, H^{12}), 7.63 – 7.35 (4H, br m, $H^{6,10,11}$), 6.94 (2H, d, *J* = 7.5, H^7), 4.71 (2H, d, *J* = 6, CH_2O), 4.59 (2H, s , CH_2O), 4.20 (2H, m), 4.14 – 4.00 (4H, br m., CH_2OCO), 3.92 (1H, br s, NH), 3.59

– 2.73 (22H, m. br., $H^{15,16,17,24,25}$), 1.38 – 1.06 (15H, br m.,$H^{1,20,23}$). **^{13}C NMR** (101 MHz, 295K, CD_3OD) δ 172.2(C^3), 160.6 (C^{21}), 151.9 (C^{18}), 150.6 (C^{12}), 134.7($C^{10,11}$), 126 (C^6), 122.4 (C^5), 119.51 ($C^{8,9}$), 116.1(C^7), 113.70, 86.0 ($C^{26,27}$), 71.5 ($C^{14,17}$), 65.8 (C^{19}), 58.0 (C^4), 49.0 ($C^{15,16,24,25}$), 47.8 ($C^{2,22}$), 17.8 (C^{20}), 9.1 ($C^{1,23}$). **MALDI-TOF MS(+)** m/z calc. for $C_{40}H_{57}N_7O_9$ 779.4218, found 779.4243.

[Eu.L^1]

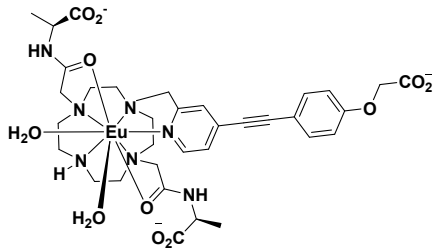

An aqueous solution of sodium hydroxide (0.4 M, 0.5 mL) was added to a solution of compound **6** (17 mg, 22 μmol) in methanol (0.5 mL). The mixture was stirred at 60 °C for 10 h. The reaction was monitored by LC-MS. Upon completion, aqueous hydrochloric acid (0.1 M) was added slowly until the pH reached 6.5. Europium chloride hexahydrate (6.5 mg, 25.3 μmol) was added and the pH was readjusted to 6.5 by addition of aqueous sodium hydroxide solution (0.1 M). The reaction was stirred at 60 °C for 24 h. The solvent was removed under reduced pressure and the resulting solid was purified by RP-HPLC. (Table 1, retention time: 9.47 min) to give the product as a colourless solid (2.5 mg, 14 %). **MALDI-TOF MS(+)** m/z 845.2272 $[M+H]^+$ ($C_{34}H_{42}EuN_7O_9{}^{153}Eu$ requires 844.2178); λ_{exc} (H_2O) = 336 nm; τ (H_2O) = 0.31 ms. τ (D_2O) = 0.78 ms, *q* = 2.

[EuL^2] and precursors

Ethyl 2-(4-iodo-3,5-dimethylphenoxy)acetate, 7 [2].

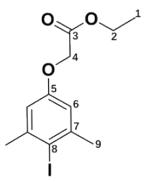

4-Iodo-3,5-dimethylphenol (5.00 g, 20.2 mmol) was dissolved in acetone (100 mL). K_2CO_3 (13.8 g, 100 mmol) and ethyl bromoacetate (2.43 mL, 22.2 mmol) were added and the reaction was heated to reflux and stirred under argon for 24 h. The mixture was filtered to remove the

potassium salts and the solvent was removed under reduced pressure. The residue was dissolved in CH_2Cl_2 (200 mL) and washed with water (200 mL). The aqueous layer was extracted into CH_2Cl_2 (3 x 200 mL) and the organic layers were combined, dried over $MgSO_4$, filtered and the solvent removed under reduced pressure. The crude solid was purified by flash column chromatography to yield **7** as a white crystalline solid (9.95 g, 98%). TLC: R_f 0.2 (silica, 5% EtOAc in hexane); **Melting point:** 73 - 74°C (Lit. 79 - 80 °C)[2]. **^{1}H NMR** (400 MHz, 295 K, $CDCl_3$) δ 6.67 (2H, s, H^6), 4.58 (2H, s, H^4), 4.27 (2H, q, *J* 7.0, H^2), 2.44 (6H, s, H^9), 1.30 (3H, t, *J* 7.0 H^1). **^{13}C NMR** (101 MHz, 295 K, $CDCl_3$) δ 168.92 (C^3), 157.50 (C^5), 143.21 (C^7), 113.61 (C^6), 98.57 (C^8), 65.45 (C^4), 61.57 (C^2), 29.91 (C^9), 14.32 (C^1).

Ethyl 2-(4-((2-(hydroxymethyl)pyridin-4-yl)ethynyl)-3,5-dimethylphenoxy)acetate, 8

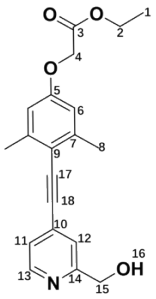

Ethyl 2-(4-iodo-3,5-dimethylphenoxy)acetate (0.98 g, 2.93 mmol) was dissolved in anhydrous THF (20 mL) and the solution was degassed (3 freeze-thaw cycles). (4-Ethynylpyridin-2-yl)methanol (0.30 g, 2.25 mmol) and DIPEA (39 mL, 0.225 mmol) were added and the solution was degassed (freeze-thaw cycle) once more. Bis(triphenylphosphine)palladium chloride (79 mg, 0.113 mmol) and cuprous iodide (43 mg, 0.225 mmol) were added and the resulting brown solution was stirred at 65 °C under argon for 24 h. The solvent was removed under reduced pressure and the resulting brown oil was purified by column chromatography to give the title compound as a pale yellow solid (94 mg, 12 %). TLC analysis R_f 0.45 (silica, 5% CH_3OH in CH_2Cl_2); **Melting point:** 97 - 99°C. **^{1}H NMR** (400 MHz, 295 K, $CDCl_3$) δ 8.53 (1H, d, *J* 7.5, H^{13}), 7.33 (1H, dd, *J* 7.5, 3.0, H^{11}), 6.65 (2H, s, H^6), 4.78 (2H, s, CH_2O), 4.63 (2H, s, CH_2O), 4.30 (2H, q, *J* 7.5, H^2), 2.48 (6H, s, H^8), 1.63 (s, 2H), 1.31 (3H, d, *J* 7.5, H^1), 1.27 (1H, br s OH). **^{13}C NMR** (101 MHz, 295 K, $CDCl_3$) δ 168.8 (C^5), 158.1 (C^3), 143.0 (C^{14}), 124.2 ($C^{11,12}$), 115.4 (C^{10}), 113.4 (C^6), 94.1 (C^{17}), 92.2 (C^{18}), 65.3 ($C^{4,15}$), 61.6 (C^2), 21.5 (C^8), 14.3 (C^1). **MALDI-TOF MS(+)** m/z calc. for $C_{17}H_{17}NO_2$ 339.1465, found 339.1520.

Ethyl (2-(4-((4-((4-(2-ethoxy-2-oxoethoxy)-2,6-dimethylphenyl)ethynyl)pyridin-2-yl)methyl)-7-(2-oxo-2-((3-oxopentan-2-yl)amino)ethyl)-1,4,7,10-tetraazacyclododecan-1-yl)acetyl)alaninate, 9

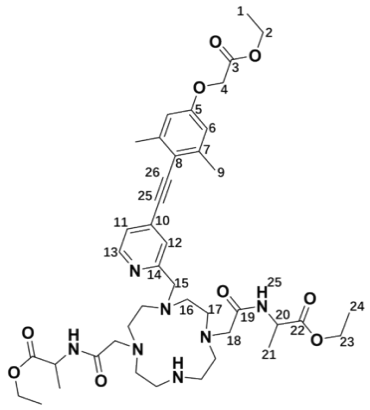

Ethyl 2-(4-((2-(hydroxymethyl)pyridin-4-yl)ethynyl)-3,5-dimethylphenoxy)acetate, **8**, (94 mg, 0.28 mmol) was dissolved in anhydrous THF (5 mL) and DIPEA (0.59 mL, 3.36 mmol) was added. The mixture was stirred at 5 °C (ice/water bath) and methanesulfonic anhydride (390 mg, 2.24 mmol) was added. The reaction was allowed to warm to room temperature and stirred under nitrogen for 12 h. The solvent was removed under reduced pressure and the residue dissolved in CH_2Cl_2 (15 mL) and washed with water (15 mL). The aqueous layer was re-extracted with CH_2Cl_2 (3 x 15 mL) and the organic layers were combined, dried over $MgSO_4$, filtered and the solvent removed under reduced pressure to yield the mesylate as a bright yellow solid (85 mg, 73%), which was used directly in the next step without further purification. TLC: R_f 0.3 (silica, 50 % EtOAc in hexane). **ESI-MS(+)** m/z calc. for $C_{21}H_{23}NO_6S$ 417.1246, found 418.132 $[M+H]^+$.

(*SS*)-Bis(ethyl-N-acetyl-*S*-alanine)-1,4,7,10- tetraazacyclododecane (45 mg, 0.10 mmol) was dissolved in dry MeCN (2 ml) and the mesylate (64 mg, 0.13 mmol) was added. DIPEA (89 µL, 0.50 mmol) was added and the mixture was stirred at 60 ˚C under argon for 24 h. The reaction was allowed to cool to room temperature. The solvent was removed under reduced pressure, and the desired product was isolated by HPLC as a light orange glassy oil (15 mg, 19 %). **^{1}H NMR** (400 MHz, 295 K, $CDCl_3$) δ 8.51 (1H, s, H^{13}), 8.49 (1H, dd, *J* 7.0 , H^{13}), 7.51 – 7.37 (4H, br m, amide NH + $H^{11,12}$), 6.63 (2H, s, H^6), 4.62 (s, 2H), 4.53 (2H, dd, *J* 7.0, H^{20}), 4.27 (4H, q, *J* 7.0, CH_2O, H^2), 4.17 – 4.00 (4H, m, H^{23}), 3.74 – 2.90 (22H, br. m, $H^{15,16,17,18}$), 2.46 (6H, s, H^9), 1.34 – 1.28 (9H, mult., $H^{21,1}$), 1.20 (6H, t, *J* 7.0, 6H, H^{24}). **^{13}C NMR** (101 MHz, 295 K, Chloroform-*d*) δ 168.8 (C^5), 158.5 (C^3), 149.5 (C^{22}), 149.0 (C^{19}), 143.4 (C^8), 134.8 (C^7), 125.8 (C^{14}), 125.7 (C^{13}), 117.2 (C^{10}), 113.48 (C^6), 94.9(C^{26}), 93.0 (C^{25}), 65.2 (C^{18}), 61.9 (C^{27}),

61.70 (C^{53}), 53.6 ($C^{16,17}$), 48.4 (C^{23}), 21.3 (C^{9}), 17.4 (C^{21}), 14.3 (C^{1}), 14.0 (C^{24}). **MALDI-TOF MS(+)** m/z calc. for $C_{42}H_{61}N_7O_9$ 807.4531, found 807.4231.

[Eu.L²]

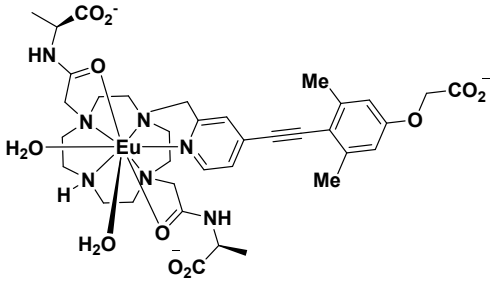

Aqueous sodium hydroxide solution (0.4 M, 0.5 mL) was added to a solution of compound **9** (15 mg, 18.6 µmol) in methanol (0.5 mL). The mixture was stirred at 60 °C for 10 h. The reaction was monitored by LC-MS, and following completion, aqueous hydrochloric acid (0.1 M) was added until pH 6.5 was achieved. Europium chloride hexahydrate (6.5 mg, 25.3 µmol) was added and the pH was readjusted to 6.5 by addition of aqueous sodium hydroxide solution (0.1 M). The reaction was stirred at 60 °C for 24 h. The solvent was removed under reduced pressure and the resulting solid was purified by RP-HPLC. (Table 2, retention time: 12.3 min) to give the product (2.5 mg, 14 %). **ESI-MS(+)** m/z calc. for $C_{36}H_{45}EuN_7O_9$ 872.2569, found 872.2663; λ_{exc} (H_2O) = 337 nm; τ (H_2O) = 0.29 ms. τ (D_2O) = 0.75 ms, q = 2.

[Eu.L³]

2-Iodo-5-methoxy-1,3-dimethylbenzene, 10 [3]

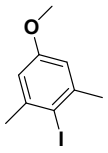

4-Iodo-3,5-dimethylphenol (1.00 g, 4.03 mmol) was dissolved in acetone (10 mL). K_2CO_3 (0.724 g, 5.24 mmol) and iodomethane (0.75 mL, 12.1 mmol) were added and the reaction was heated to reflux and stirred under argon for 24 h. The mixture was filtered to remove the potassium salts and the solvent was removed under reduced pressure. The residue was dissolved in CH_2Cl_2 (50 mL) and washed with water (50 mL). The aqueous layer was extracted into CH_2Cl_2 (3 x 50 mL) and the organic layers were combined, dried over $MgSO_4$, filtered and

the solvent removed under reduced pressure. The crude solid was purified by flash column chromatography (silica, 2% CH_2Cl_2 in hexane) to yield 10 as a white crystalline solid (1.01 g, 87%). TLC analysis Rf 0.23 (silica, 4% CH_2Cl_2 in hexane); **Melting point:** 35-36 °C (lit. 36-37 °C) [3]; **^{1}H NMR** (400 MHz, 295 K, $CDCl_3$) δ_H 6.67 (2H, s, Ar- H), 3.77 (3H, s, OCH3), 2.45 (6H, s, CH3); **^{13}C NMR** (100 MHz, 295 K, $CDCl_3$) δ_C 159.98 (Ar-C1), 142.66 (Ar-C), 112.69 (Ar-C), 96.85 (Ar-C), 55.08 (OCH_3), 29.56 (CH_3).

(4-((4-Methoxy-2,6-dimethylphenyl)ethynyl)pyridin-2-yl)methanol, 11

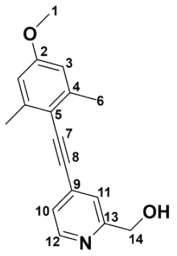

2-Iodo-5-methoxy-1,3-dimethylbenzene (**10**) (0.5 g, 1.91 mmol) was dissolved in anhydrous THF (20 mL) and the solution was degassed (three freeze-thaw cycles). (4-Ethynylpyridin-2-yl)methanol (0.19 g, 1.47 mmol) and DIPEA (5.2 mL, 2.93 mmol) were added and the solution was degassed once more. Bis(triphenylphosphine)palladium chloride (30 mg, 44 µmol) and cuprous iodide (16 mg, 88 µmol) were added and the resulting brown solution was stirred at 65 °C under argon for 24 h. The solvent was removed under reduced pressure and the resulting brown oil was purified by column chromatography to give the title compound as a white solid (203 mg, 40%). Rf 0.25 (silica, 3 % CH_3OH in CH_2Cl_2); **Melting point:** 126 - 128 °C. **^{1}H NMR** (600 MHz, 295 K, $CDCl_3$) δ 8.54 (br s, 1H, H^{12}), 7.26 (m, 2H, $H^{10,11}$), 6.63 (s, 2H, H^3), 4.79 (br s, 2H, H^{14}), 3.81 (s, 3H, H^1), 2.48 (s, 6H, H^6). **^{13}C NMR** (151 MHz, 295 K, $CDCl_3$) δ 160.0 (C^2), 142.8 (C^5), 133.0 (C^{13}), 132.3 (C^{11}), 132.2 (C^{10}), 128.7 (C^{12}), 114.3 (C^9), 112.8 (C^3), 92.6 ($C^{7,8}$), 55.4 (C^1), 21.5 (C^6). **MALDI-TOF(+)** m/z calc. for $C_{17}H_{17}NO_2$ 267.1254, found 267.1228.

Diethyl 2,2'-((2,2'-(4-((4-((4-methoxy-2,6-dimethylphenyl)ethynyl)pyridin-2-yl)methyl)-1,4,7,10-tetraazacyclododecane-1,7-diyl)bis(acetyl))bis(azanediyl))dipropionate, 12

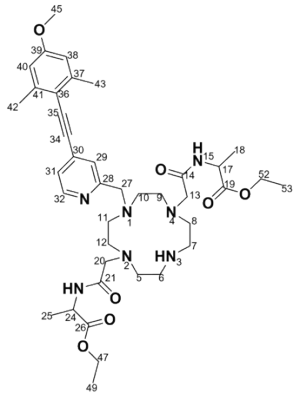

(4-((4-Methoxy-2,6-dimethylphenyl)ethynyl)pyridin-2-yl)methanol (90 mg, 0.34 mmol) was dissolved in anhydrous THF (5 mL) and DIPEA (0.72 mL,4.04 mmol) was added. The mixture was stirred at 5 °C (ice/water bath) and methanesulfonic anhydride 470 mg, 2.70 mmol) was added. The reaction was allowed to warm to room temperature and stirred under nitrogen for 12 h. The solvent was removed under reduced pressure and the residue dissolved in CH_2Cl_2 (15 mL) and washed with water (15 mL). The aqueous layer was re-extracted with CH_2Cl_2 (3 x 15 mL) and the organic layers were combined, dried over $MgSO_4$, filtered and the solvent removed under reduced pressure to yield the mesylate as a bright yellow solid (85 mg, 73%), which was used directly in the next step without further purification. TLC: Rf 0.3 (silica, 50 % EtOAc in hexane). **ESI-MS(+)** m/z calc. for $C_{18}H_{19}NO_4S$ 345.1034, found 345.1040

(SS)-Bis(ethyl-N-acetyl-S-alanine)-1,4,7,10- tetraazacyclododecane (25 mg, 0.05 mmol) was dissolved in dry MeCN (2 ml) and the mesylate (17 mg, 0.05 mmol) was added. DIPEA (27 µL, 0.15 mmol) was added and the mixture was stirred at 60 ˚C under argon for 24 h. The reaction was allowed to cool to room temperature. The solvent was removed under reduced pressure, and the desired product was isolated by HPLC as a light orange glassy oil (15 mg, 19 %).**^{1}H NMR** (400 MHz, $CDCl_3$, 295 K) δ 8.49 (d, *J* 5.0, 1H, H^{32}), 7.47 (s, 1H, H^{29}), 7.41 (d, *J* 5.0, 1H, H^{31}), 6.63 (s, 2H, $H^{38,40}$), 4.58 (d, *J* 7.0, 2H, $H^{17,24}$), 4.08 (t, *J* 7.0, 4H, $H^{47,52}$), 3.80 (s, 3H, H^{45}), 3.78 – 2.79 (m, 20H), 2.46 (s, 6H, $H^{42,43}$), 1.29 (d, *J* 7.0, 6H, $H^{18,25}$), 1.20 (t, *J* 7.0 6H, $H^{53,49}$). **^{13}C NMR** (101 MHz, 295 K, $CDCl_3$) δ 170.7 (C^{39}), 149.4 ($C^{14,21}$), 148.8 ($C^{19,26}$), 143.3 (C^{36}), 135.3 ($C^{37,41}$), 125.9 (C^{32}), 125.7 (C^{28}), 117.19 (C^{30}), 114.3 (C^{31}), 113.6 (C^{29}), 112.9 ($C^{38,40}$), 95.8 (C^{35}), 92.8 (C^{34}), 61.9 (C^{27}), 56.9 ($C^{13,20}$), 55.4 (C^{45}), 52.0 (cyclen), 48.4 ($C^{52,47}$), 42.9 ($C^{17,24}$), 21.3 ($C^{42.43}$), 17.3 ($C^{18,25}$), 14.0 ($C^{49,53}$). **MALDI-TOF MS(+)** m/z calc. for $C_{35}H_{57}N_7O_7$ 735.4319, found 735.4313;

$[EuL_3]^+$

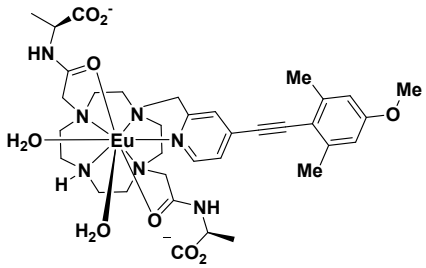

An aqueous solution of sodium hydroxide (0.4 M, 0.5 mL) was added to a solution of compound **12** (10 mg, 17 μmol) in methanol (0.5 mL). The mixture was stirred at 60 °C for 10 h. The reaction was monitored by LC-MS. MALDI-TOF MS(+) m/z calc. for $C_{35}H_{49}N_7O_7$. 679.3766, found $[M+H]^+$ 680.4130; Upon completion, aqueous hydrochloric acid (0.1 M) was added slowly until the pH reached 6.5. Europium chloride hexahydrate (6.5 mg, 25.3 μmol) was added and the pH readjusted to 6.5 by addition of aqueous sodium hydroxide solution (0.1 M). The reaction was stirred at 60 °C for 24 h. The solvent was removed under reduced pressure and the resulting solid was purified by RP-HPLC. (Table 3, t_R 16.0 min) to give the product as a colourless solid (5.3 mg, 38 %). **MALDI-TOF (ESI$^+$)** m/z 830.2662 ($C_{35}H_{46}EuN_7O_7$ ^{153}Eu requires 830.2671); λ_{exc} (H_2O) = 337 nm; τ (H_2O) = 0.27 ms. τ (D_2O) = 0.59 ms, q = 2.

References

1. D. G. Smith, G.-l. Law, B. S. Murray, R. Pal, D. Parker, K.-L. Wong, *Chem. Commun.* 2011, **47**, 7347-7349.
2. M. Starck, R. Pal, D. Parker, *Chemistry-a European Journal* 2016, **22**, 570-580.
3. E. R. Neil, D. Parker, *RSC Advances* 2017, **7**, 4531-4540.
4. R. Carr, N. H. Evans and D. Parker, *Chem. Soc. Rev*., 2012, **41**, 7673-7686; D. Parker, J. D. Fradgley and K-L. Wong, *Chem Soc Rev*., 2021, **50**, 8193-8213.
5. P. Atkinson, Y. Bretonniere, D. Parker, *Chem. Commun*., 2004, 438-9; P. Atkinson, Y. Bretonniere, G. Muller and D. Parker, *Helv. Chim.Acta*, 2005, **88**, 391-405; P. Atkinson, B. S. Murray and D. Parker, *Org. Biomol. Chem*., 2006, **4**, 3166-3172.
6. E. R. Neil, M. A. Fox, R. Pal, L-O Palsson, B. A. O'Sullivan and D. Parker, *Dalton Trans*. 2015, **44**, 14937-14951; E. R. Neil, M. A. Fox, R Pal and D Parker, *Dalton Trans* 2016, **45**, 8355
7. J. Reinders and A. Sickmann, *Proteomics*, 2007, **5**, 4052-4061; J. L. Wang, Y. J. Zhang, H. Jiang, Y. Cai and X. H. Qian, *Proteomics*, 2006, **6**, 404-11.
8. L. Trojer, G. Stecher, I. Feuerstein, S. Lubbad and G. K. Bonn, *J. Chromatogr.A*, 2005, **1079**, 197-207; J. N. M. Ballard, G. A. Lajoie, K. K. C. Yeung, *J. Chromatogr. A,* 2007, 1156, 101-110; O. N. Jensen, E. Sachon, S. Mohammed and N. Bache, *Rapid Comms. Mass Spectrom*., 2006, **20**, 1127-1134.

9. A. Motoyama, T. Xu, C. I. Ruse, J. A. Wohlschlegel, and J. R. Yates, *Anal. Chem*., 2007, **79**, 3623-3634.
10. I. Kuroda, Y. Shintani, M. Motokawa, S. Abe and M. Furuno, *Anal. Sci*., 2004, **20**, 1313-1319.
11. M. Starck, J. D. Fradgley, S. Di Vita, J. A. Mosely, R. Pal and D. Parker, *Bioconjugate Chem*. 2020, **31**, 229-240.
12. R. Carr, R. Puckrin, B.K. McMahon, R. Pal, D. Parker, L.O. Pålsson. *Methods Appl Fluoresc,* **2014**, 2(2):024007.
13. P. Pongprayoon, N. Kuntip, T. Suwanasopee, D. Jattawa, J. Niramitranon, D. Japrung, S. Koonawootrittriron, *Journal of biomolecular structure & dynamics*, **2023**, *43*(6), 2772–2780.

NMR Spectra

^{1}H NMR spectrum ($CDCl_3$, 400 MHz, 295 K) N-Bromoacetyl-(S)-alanine ethyl ester, 1

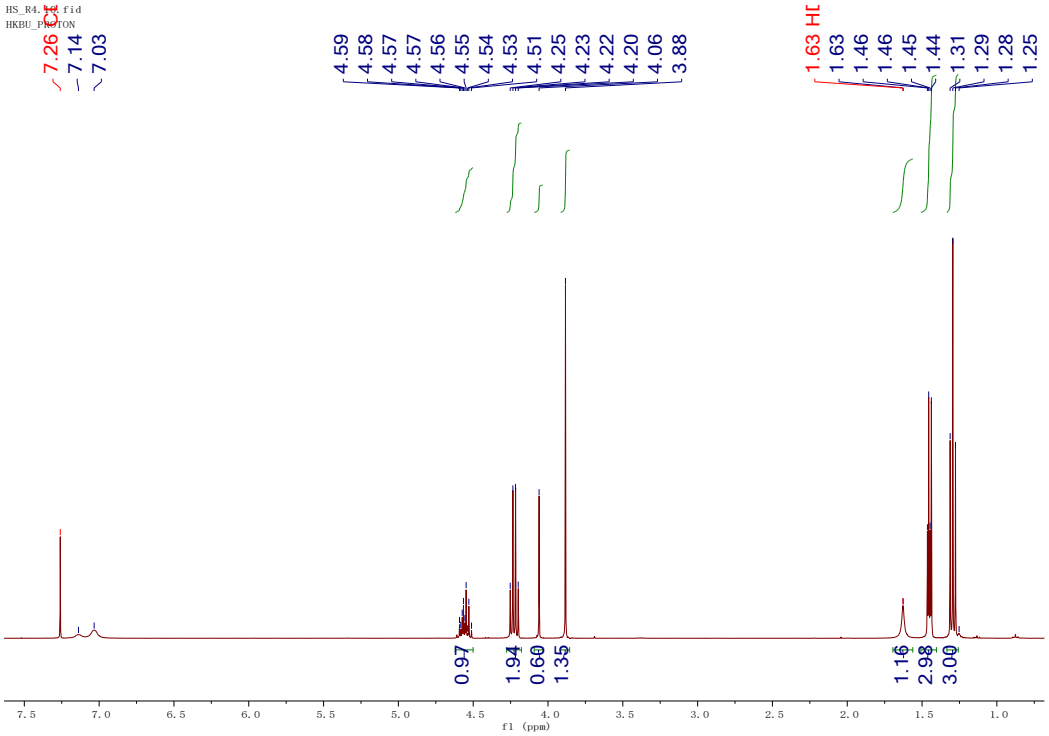

^{13}C NMR spectrum ($CDCl_3$, 400 MHz, 295 K) of N-Bromoacetyl-(S)-alanine ethyl ester, 1

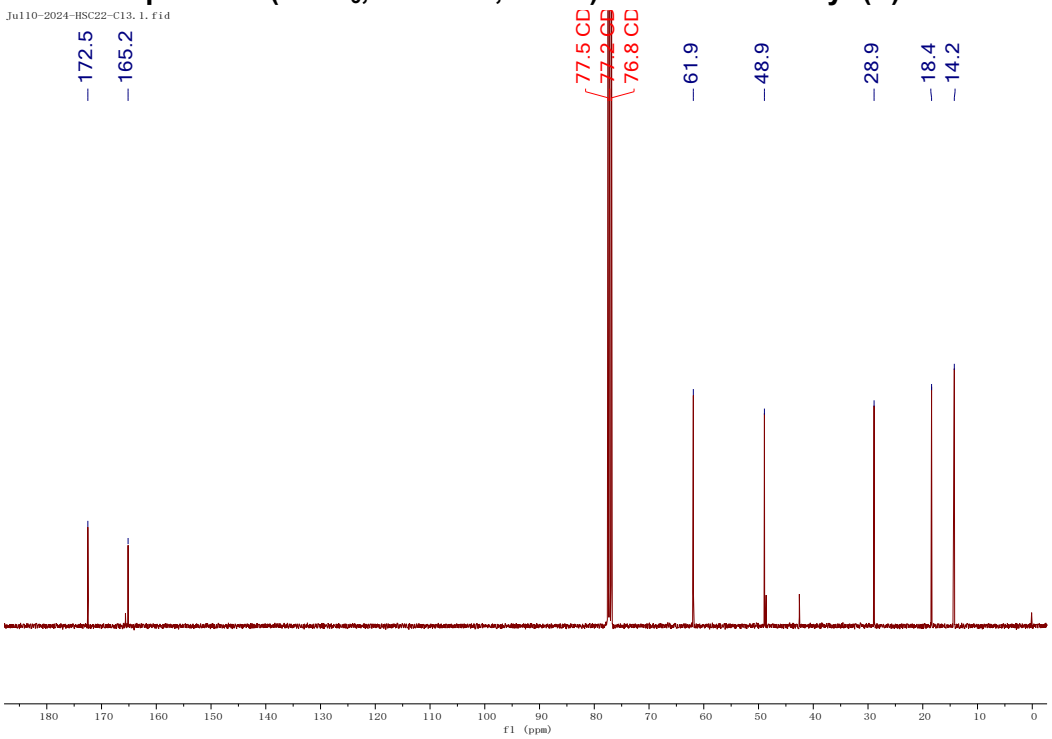

^{1}H NMR spectrum ($CDCl_3$, 400 MHz, 295 K) of compound 2

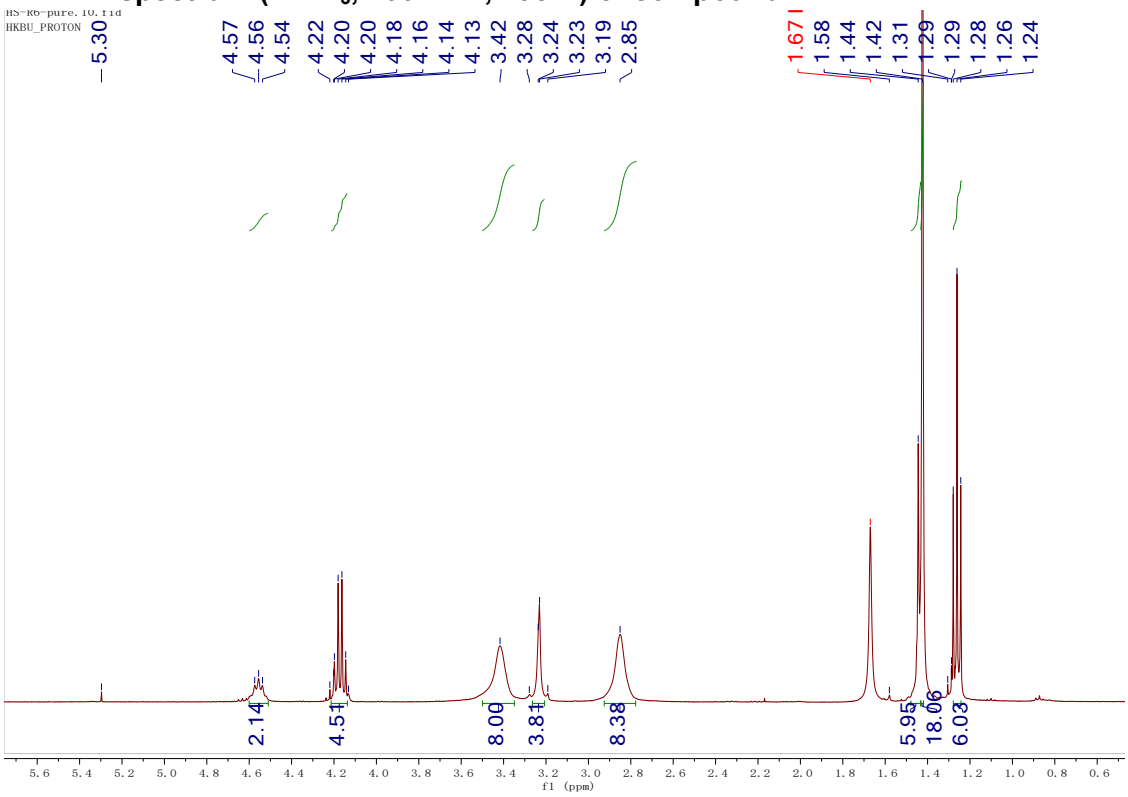

^{13}C NMR spectrum ($CDCl_3$, 400 MHz, 295 K) of compound 2

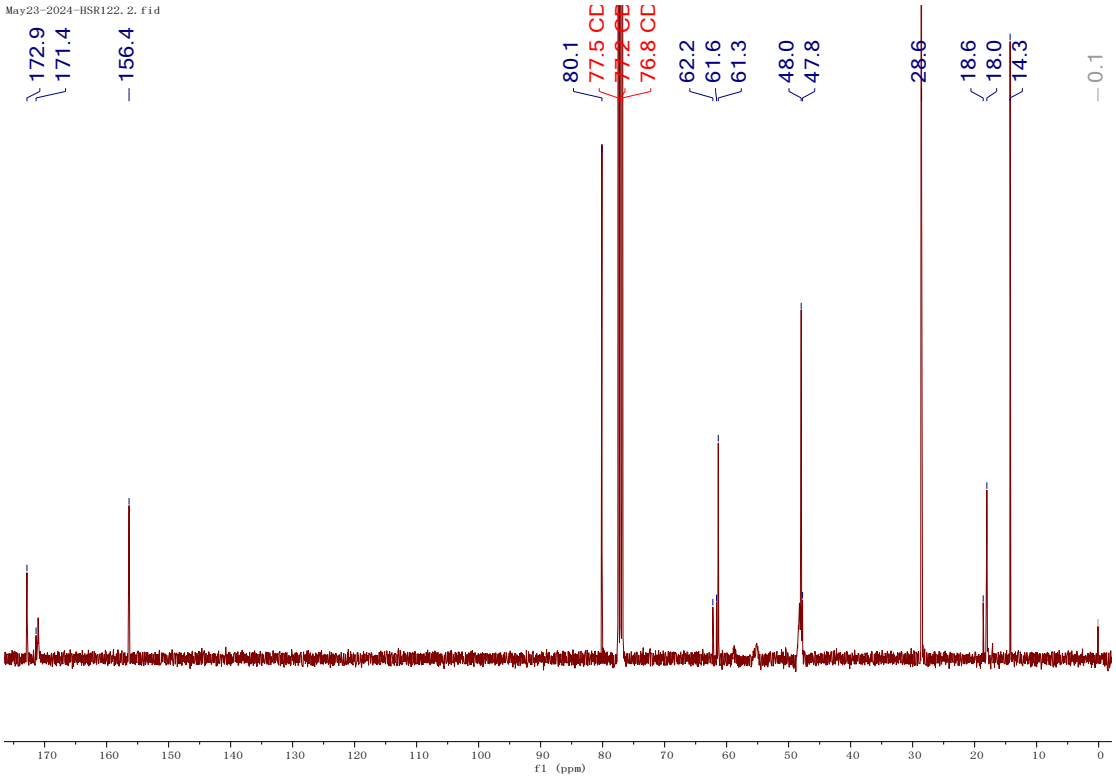

^{1}H NMR spectrum (CD_3OD, 400 MHz, 295 K) of compound 3

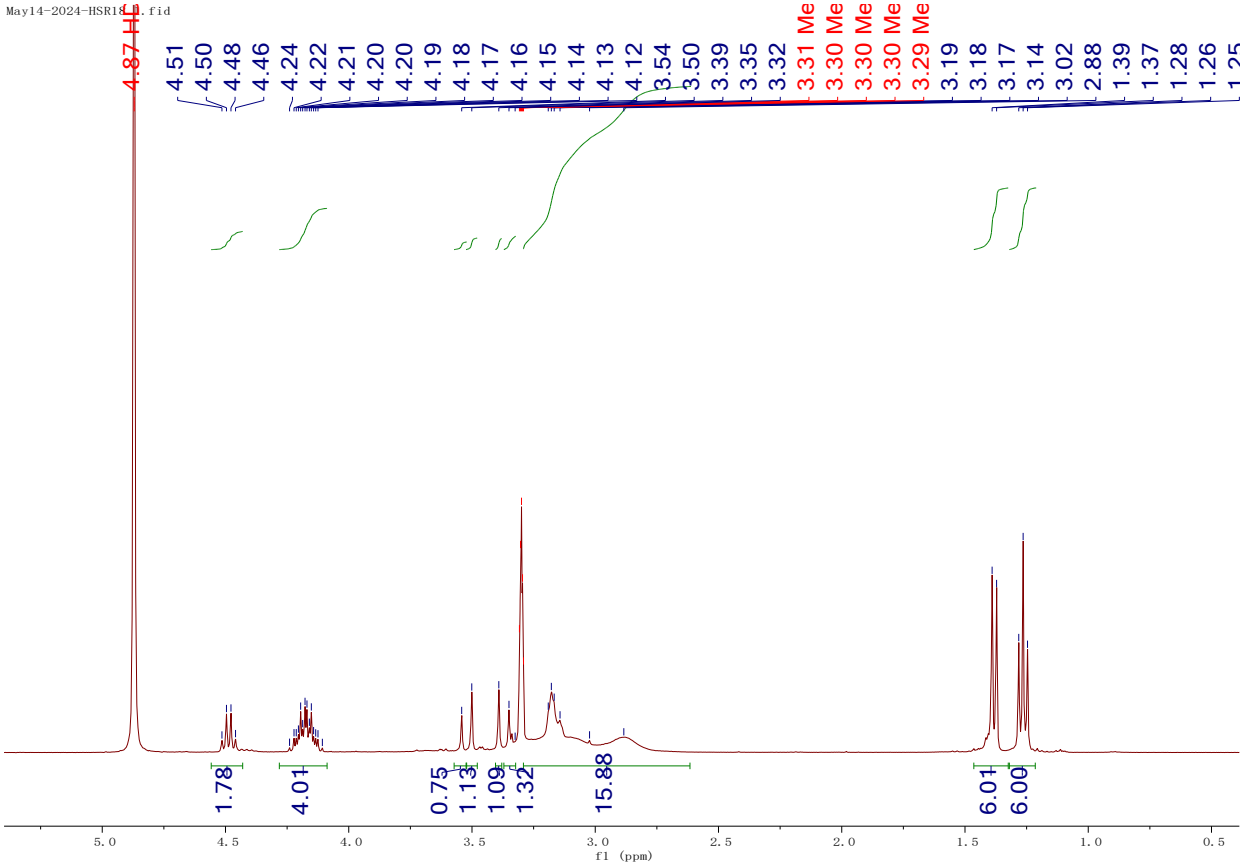

^{13}C NMR spectrum (CD_3OD, 400 MHz, 295 K) of compound 3

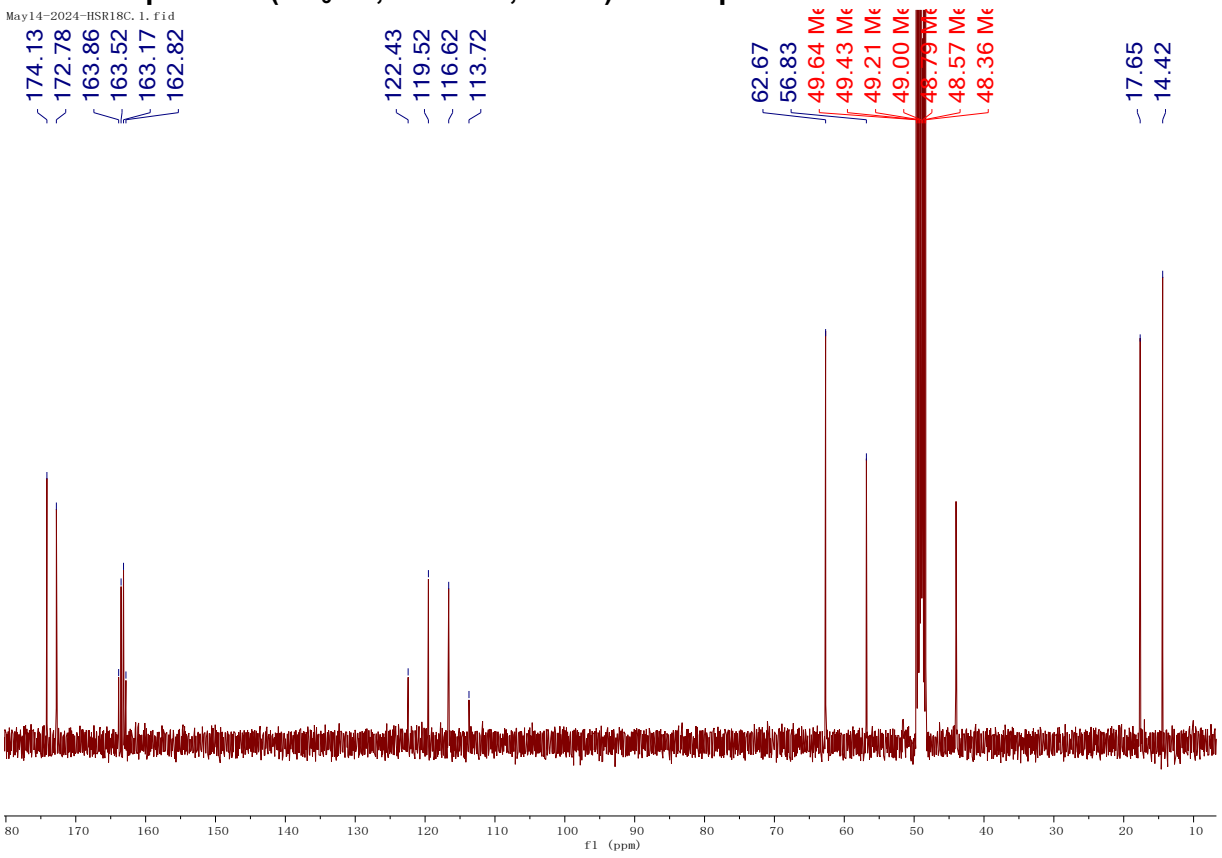

^{1}H NMR spectrum ($CDCl_3$, 400 MHz, 295 K) of Ethyl 2-(4-iodophenoxy)acetate, 4

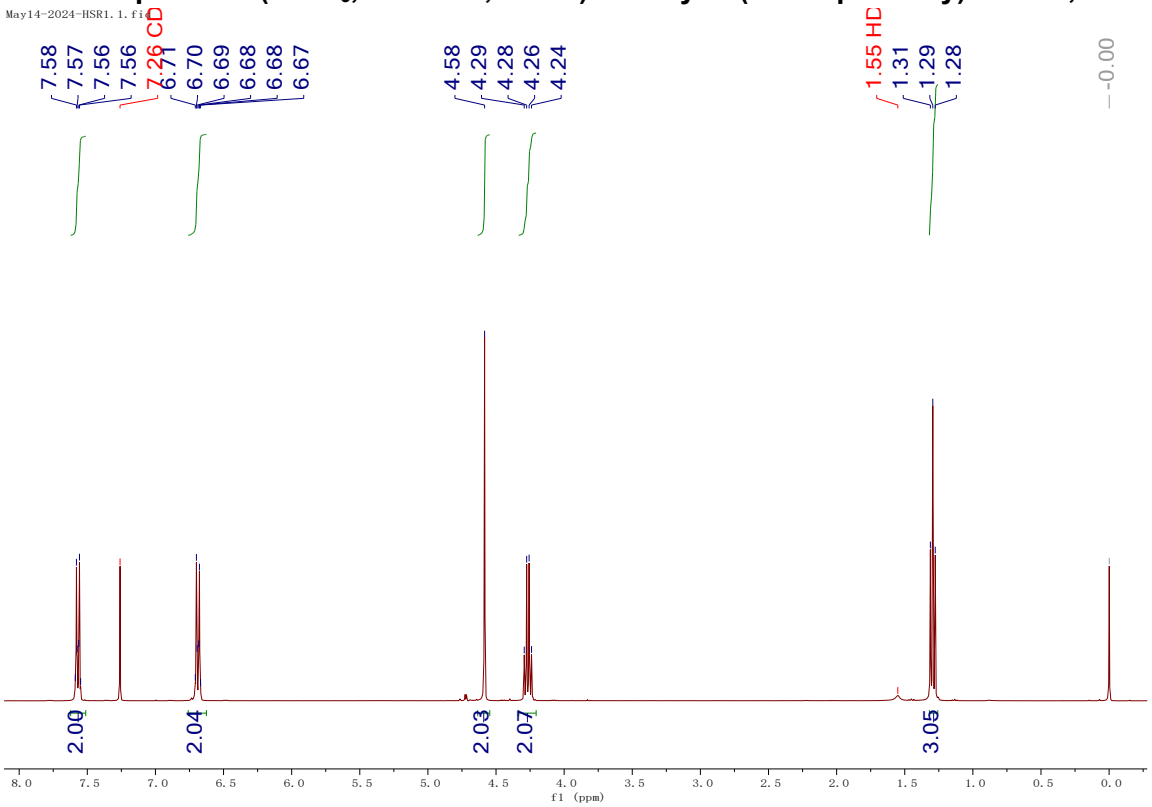

^{13}C NMR spectrum ($CDCl_3$, 400 MHz, 295 K) of Ethyl 2-(4-iodophenoxy)acetate, 4

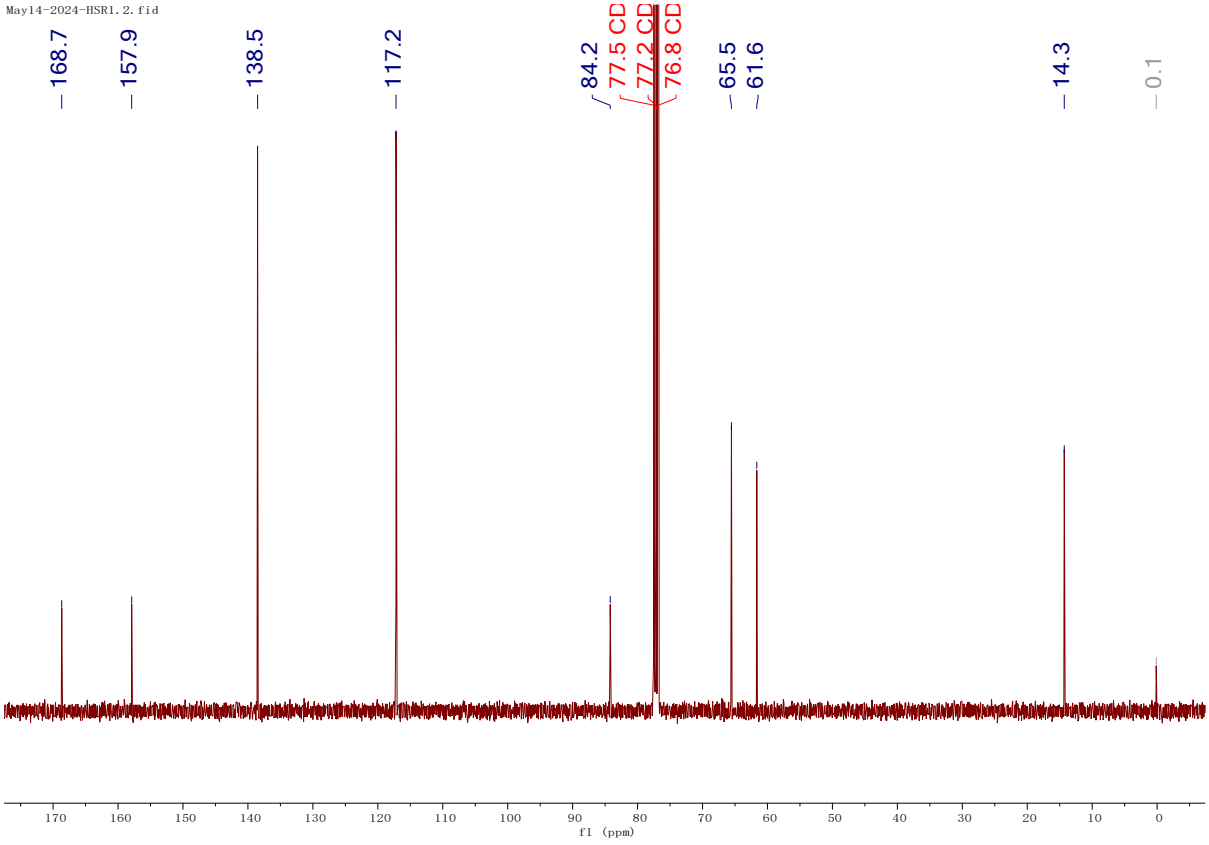

^{1}H NMR spectrum ($CDCl_3$, 400 MHz, 295 K) of ethyl 2-(4-((2-(hydroxymethyl)pyridin-4-yl)ethynyl)phenoxy)acetate, 5

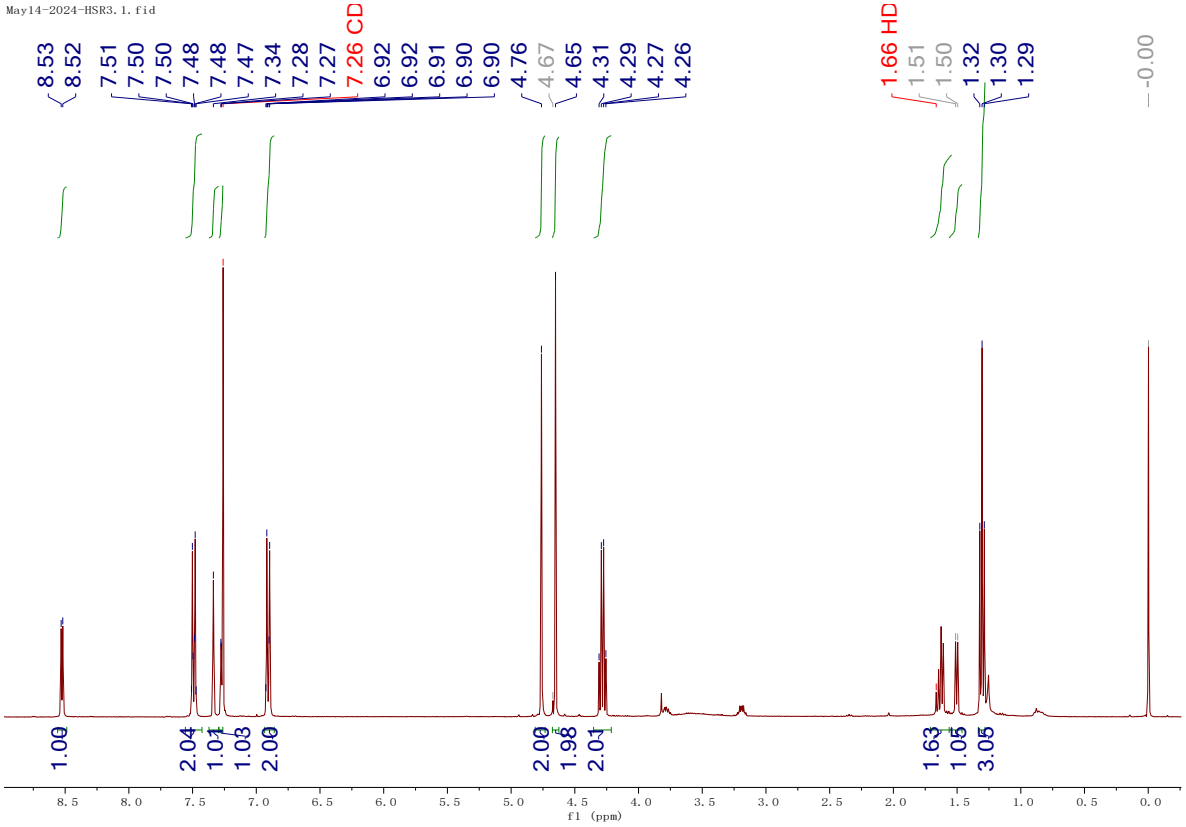

^{13}C NMR spectrum ($CDCl_3$, 400 MHz, 295 K) of ethyl 2-(4-((2-(hydroxymethyl)pyridin-4-yl)ethynyl)phenoxy)acetate, 5

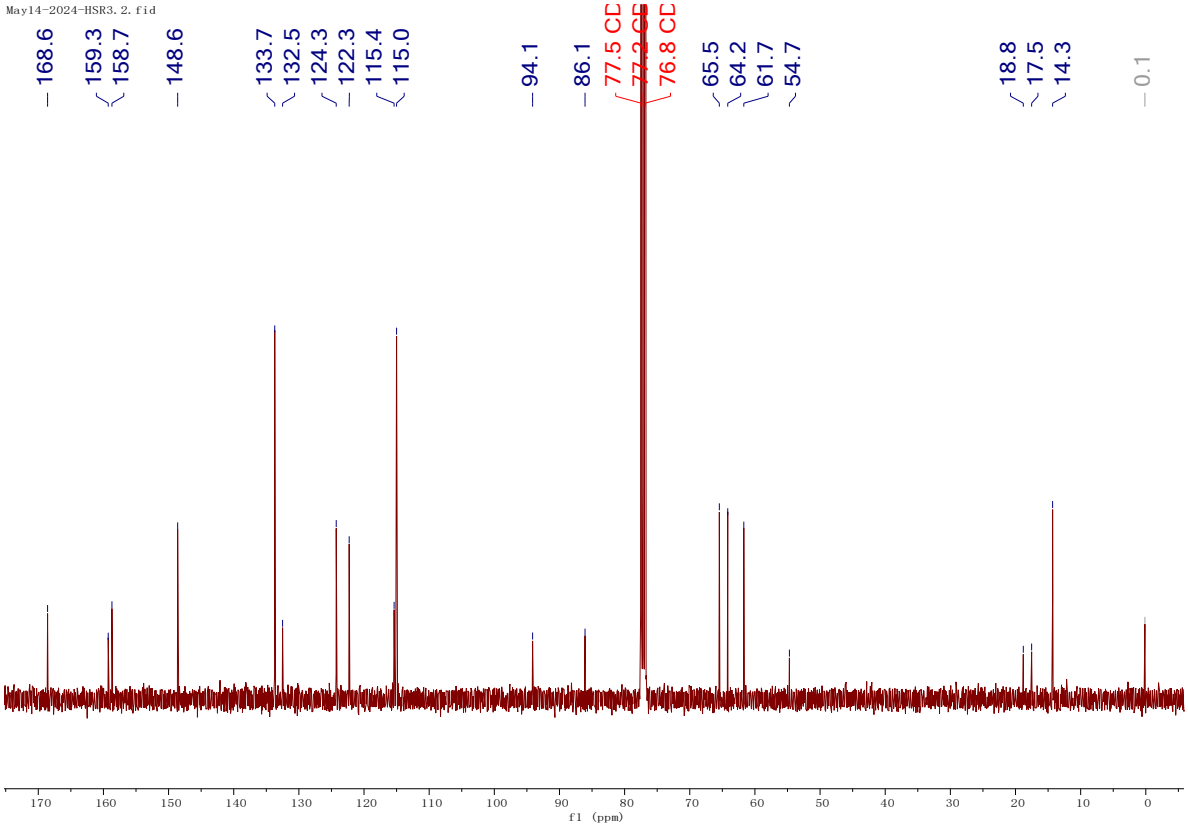

^{1}H NMR spectrum (CD_3OD, 400 MHz, 295 K) of compound 6

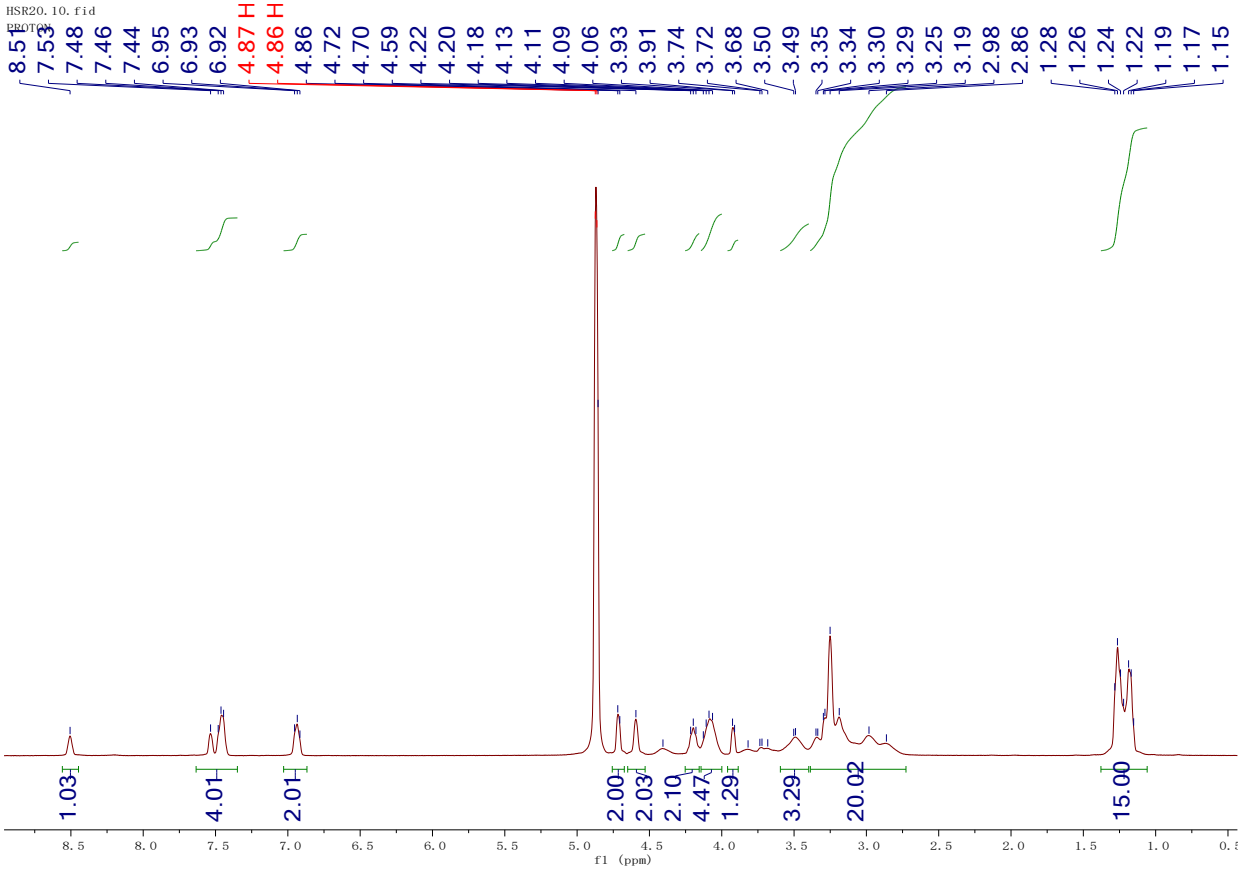

^{13}C NMR spectrum (MeOD, 400 MHz, 295 K) of compound 6

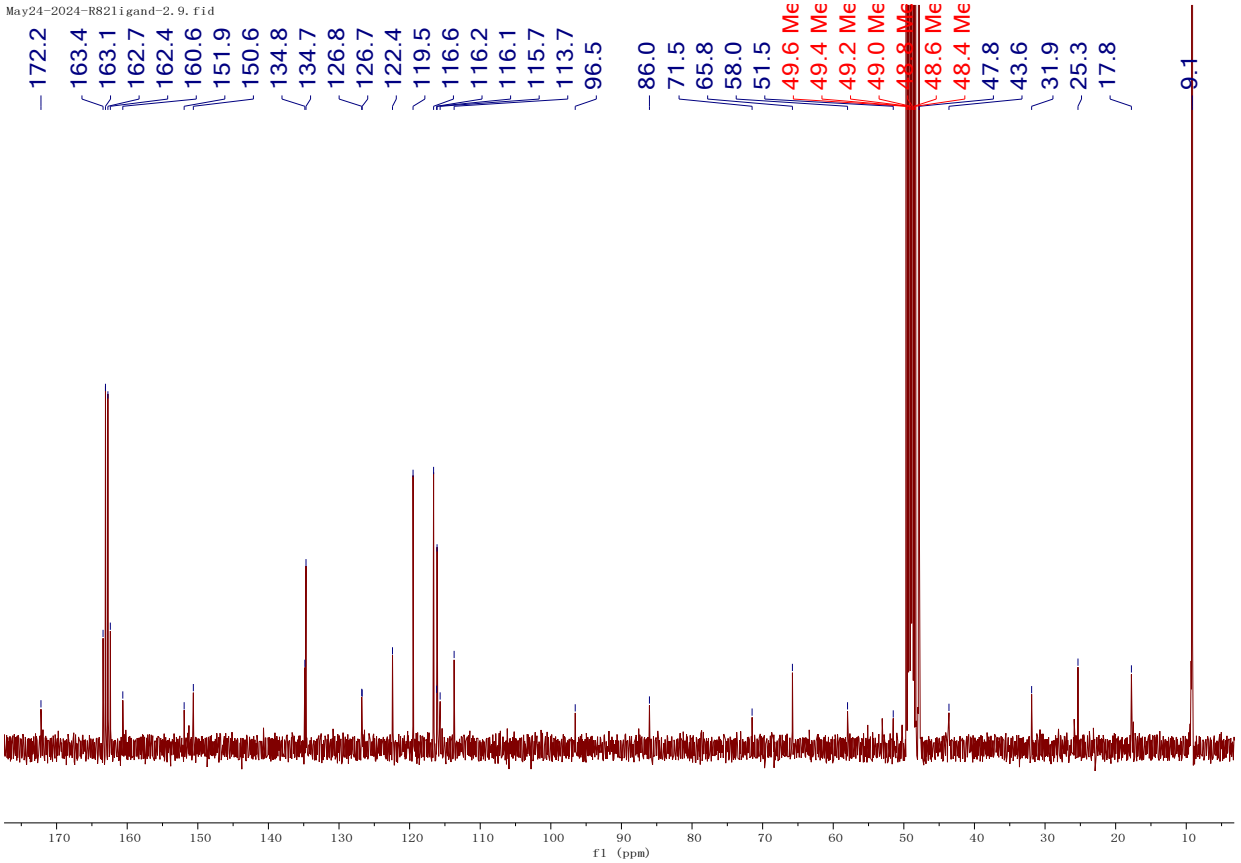

^{1}H NMR spectrum ($CDCl_3$, 400 MHz, 295 K) of ethyl 2-(4-iodo-3,5-dimethylphenoxy)acetate, 7

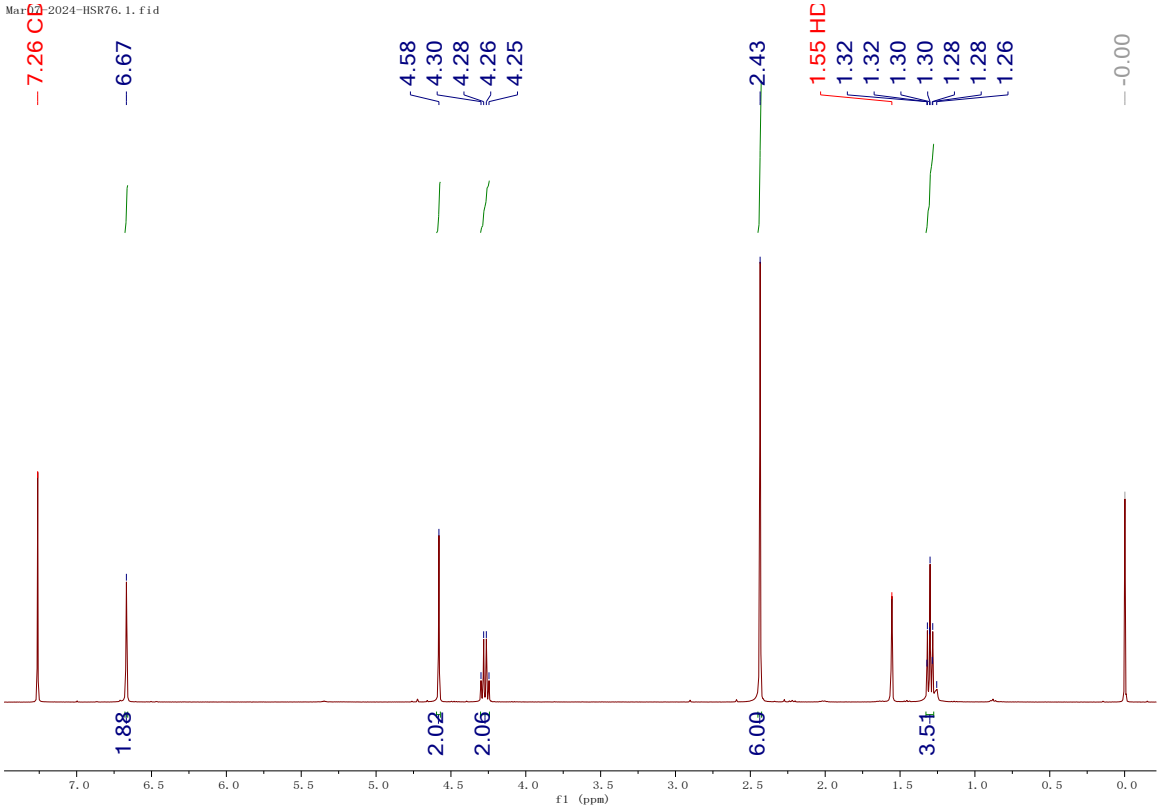

^{13}C NMR spectrum ($CDCl_3$, 400 MHz, 295 K) of ethyl 2-(4-iodo-3,5-dimethylphenoxy)acetate, 7

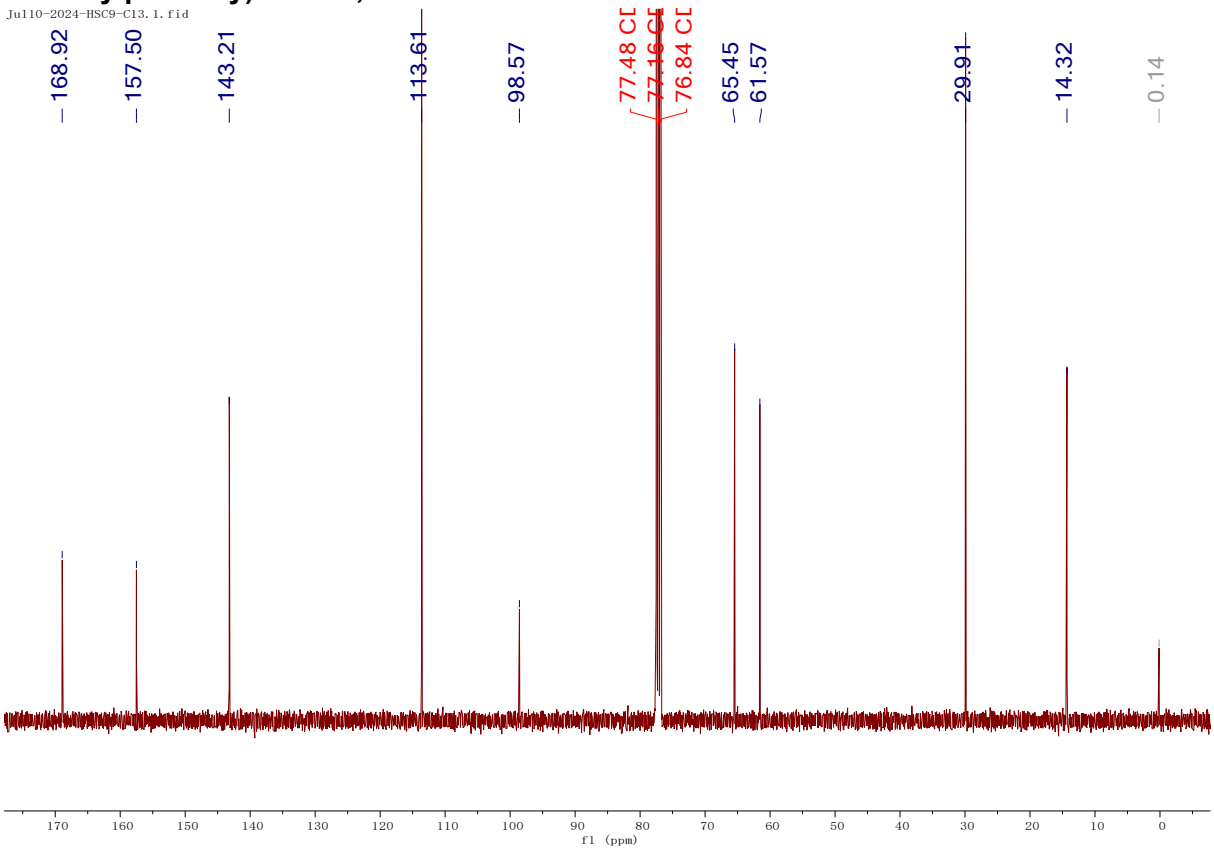

^{1}H NMR spectrum ($CDCl_3$, 400 MHz, 295 K) of ethyl 2-(4-((2-(hydroxymethyl)pyridin-4-yl)ethynyl)-3,5-dimethylphenoxy)acetate, 8

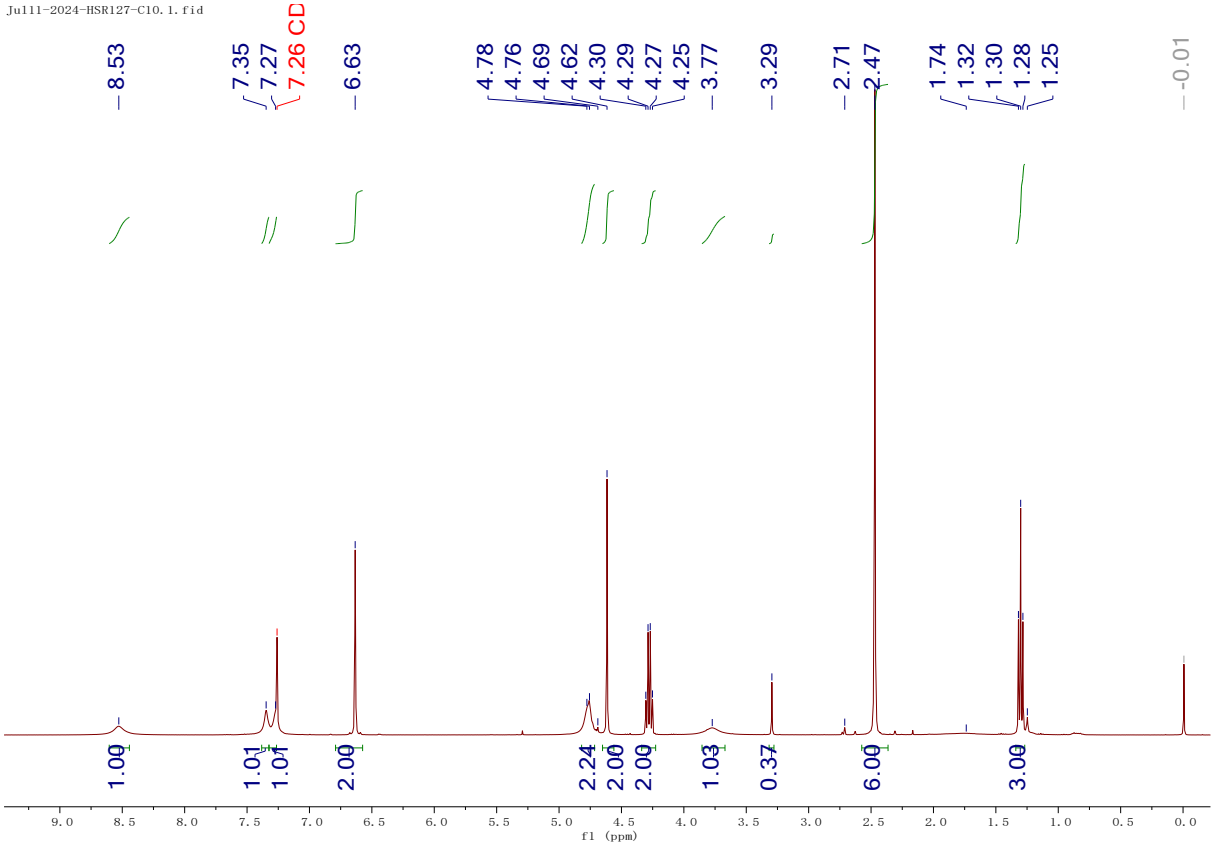

^{13}C NMR spectrum ($CDCl_3$, 400 MHz, 295 K) of ethyl 2-(4-((2-(hydroxymethyl)pyridin-4-yl)ethynyl)-3,5-dimethylphenoxy)acetate, 8

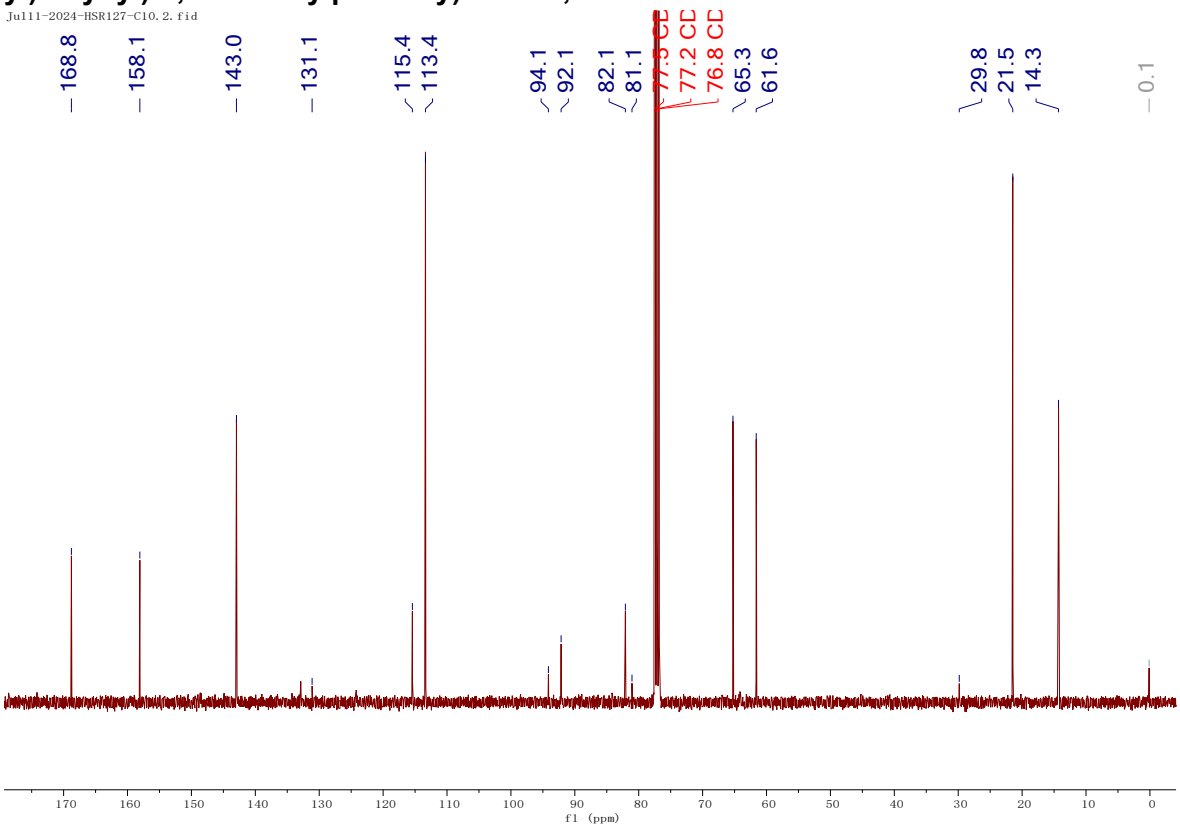

^{1}H NMR spectrum ($CDCl_3$, 400 MHz, 295 K) of compound 9

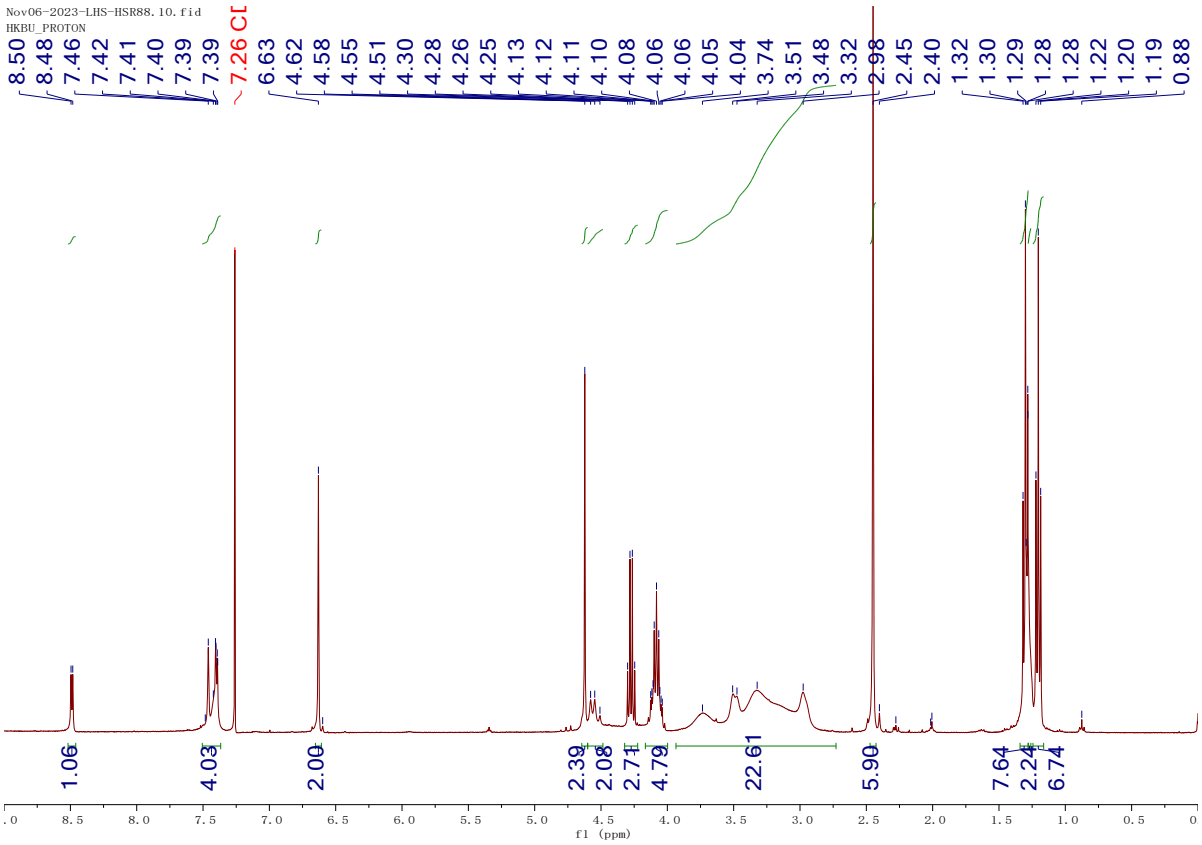

^{13}C NMR spectrum ($CDCl_3$, 400 MHz, 295 K) of compound 9

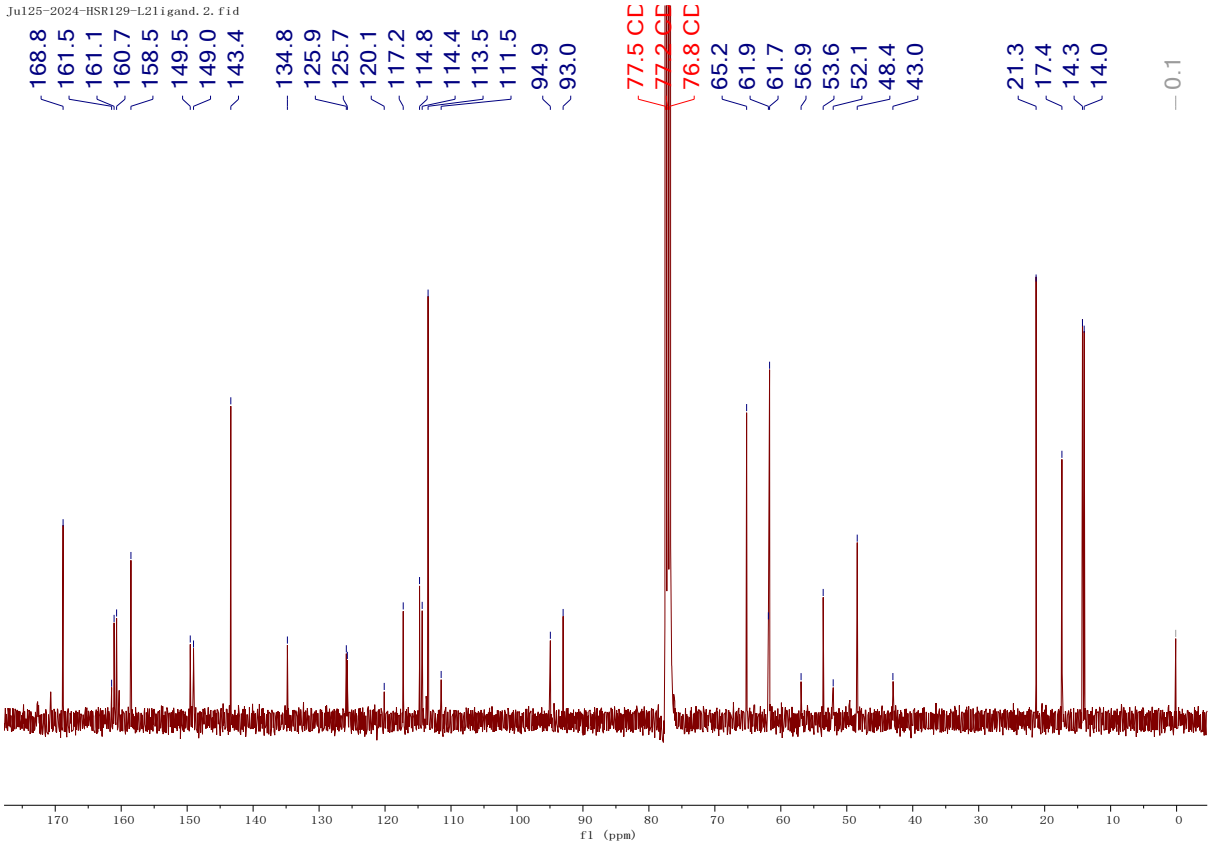

^{1}H NMR spectrum ($CDCl_3$, 400 MHz, 295 K) of 2-iodo-5-methoxy-1,3-dimethylbenzene,

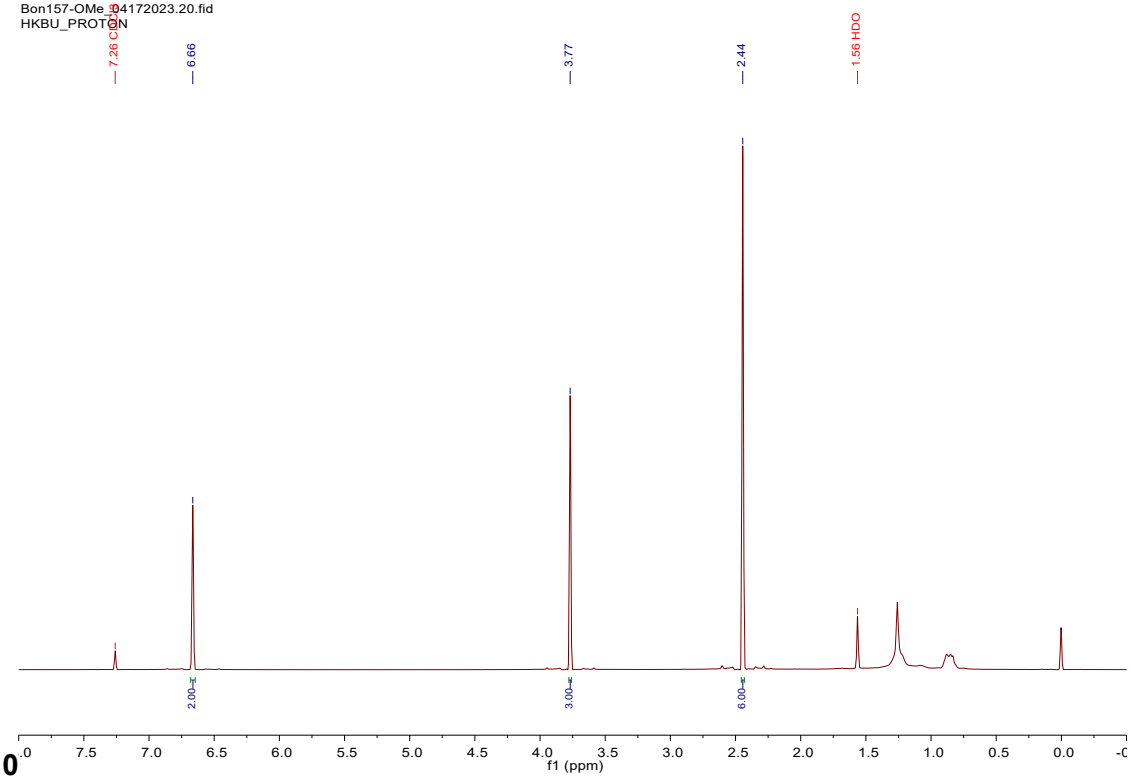

10

^{13}C NMR spectrum ($CDCl_3$, 400 MHz, 295 K) of 2-iodo-5-methoxy-1,3-dimethylbenzene,

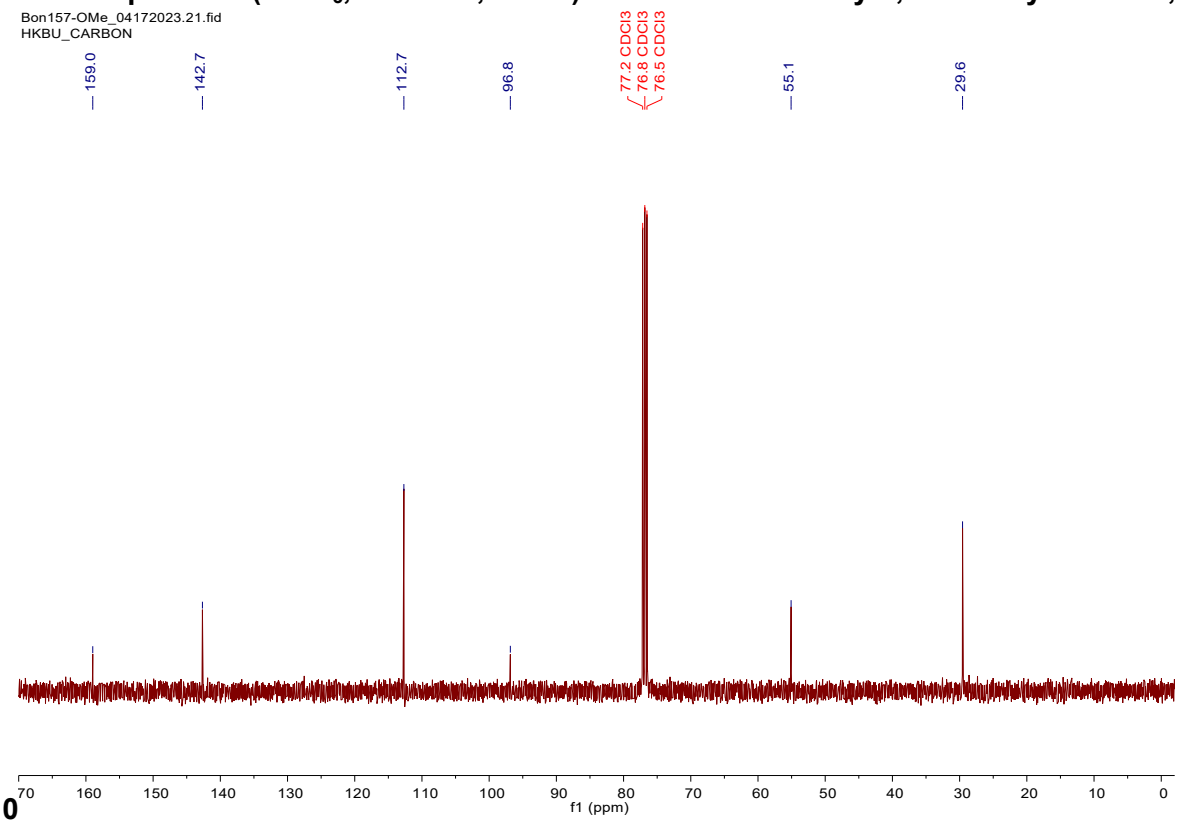

10

^{1}H NMR spectrum ($CDCl_3$, 600 MHz, 295 K) of (4-((4-methoxy-2,6-dimethylphenyl)ethynyl)pyridin-2-yl)methanol, 11

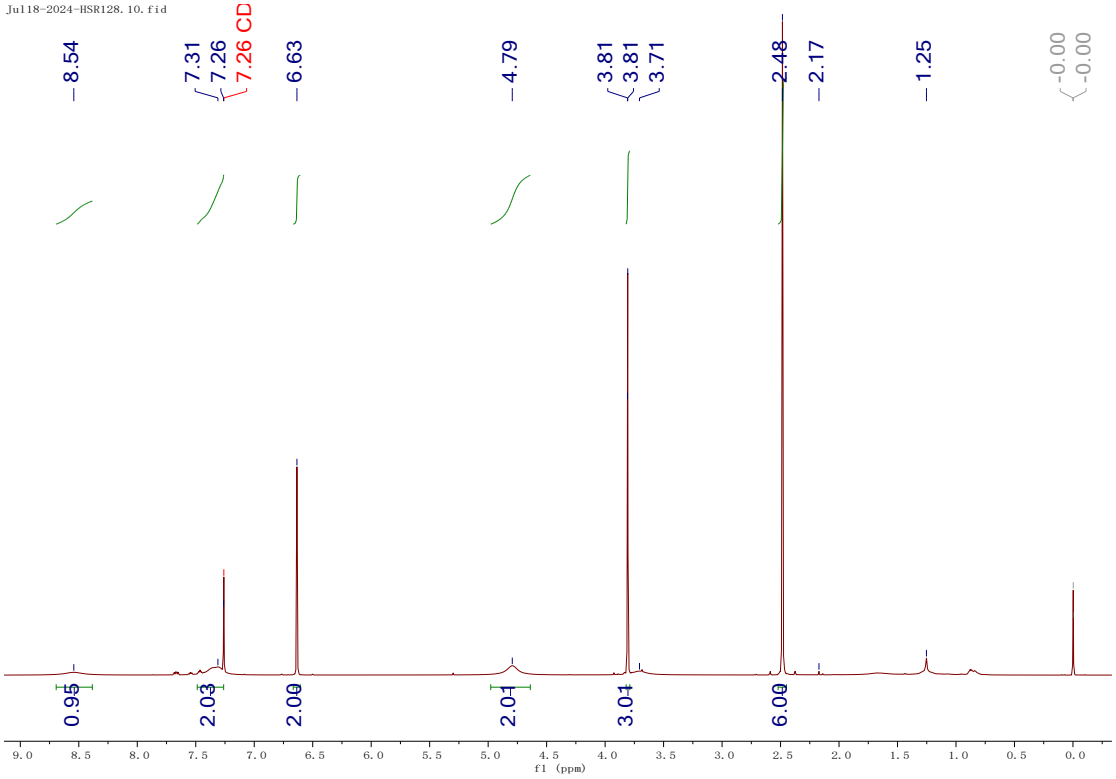

^{13}C NMR spectrum ($CDCl_3$, 151 MHz, 295 K) of (4-((4-methoxy-2,6-dimethylphenyl)ethynyl)pyridin-2-yl)methanol, 11

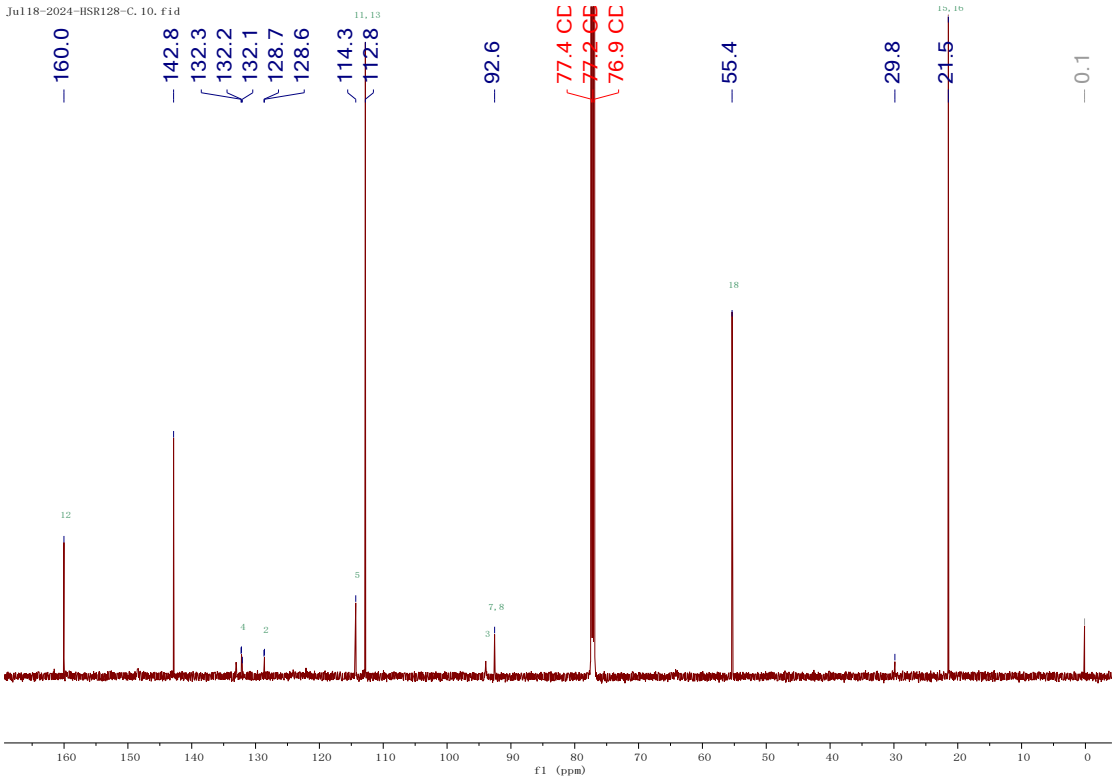

^{1}H NMR spectrum ($CDCl_3$, 400 MHz, 295 K) of compound 12

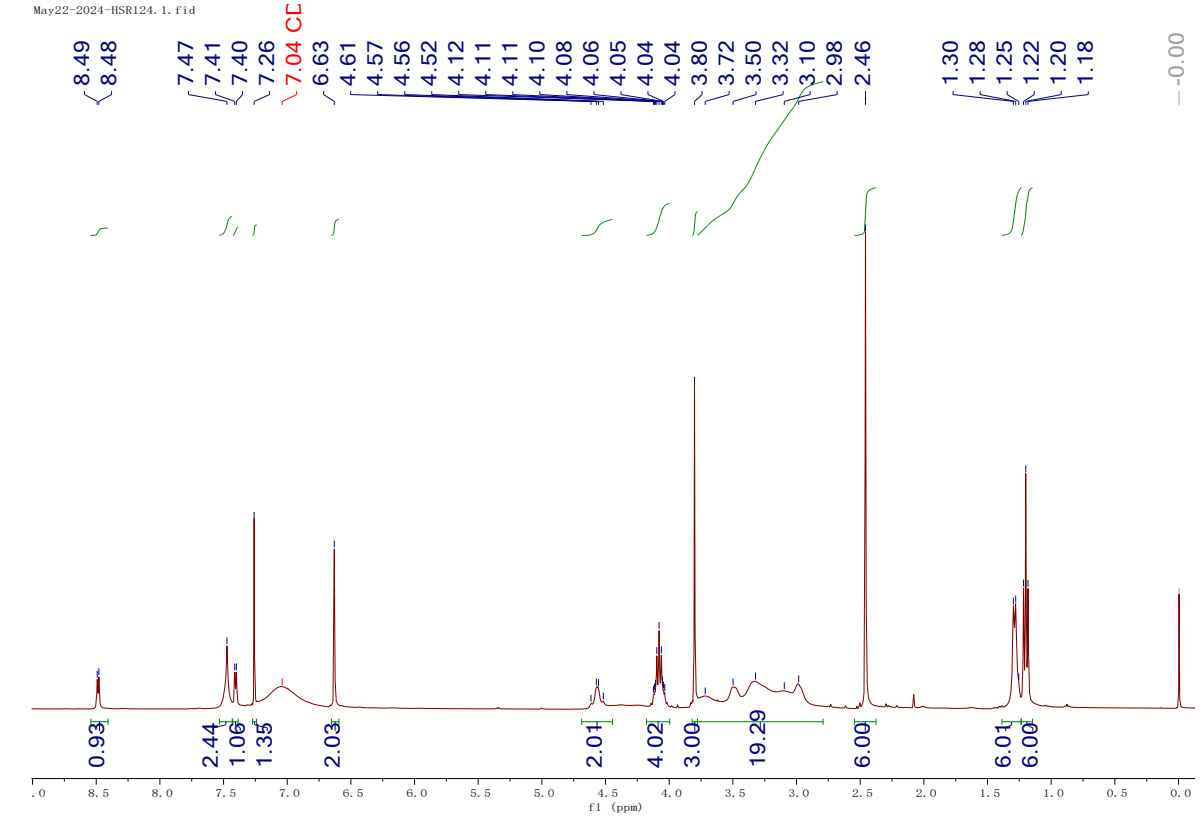

^{13}C NMR spectrum ($CDCl_3$, 400 MHz, 295 K) of compound 12